UAV Trajectory, Power and User-Association Optimization for Covert Communications in ICRNs

Riyu Wang, Bin Yang, Shikai Shen, Yumei She, Fei Deng, Kaiguo Qian, Tarik Taleb

***Abstract*—This paper studies covert communications in an unmanned aerial vehicle (UAV)-assisted interweave cognitive radio network (ICRN). Specifically, a secondary user (UAV) opportunistically utilizes the idle spectrum resource of a primary user (Warden) to covertly transmit short-packets to ground receivers (GRs), while Warden tries to detect the existence of the UAV covert communications. To ensure fairness of covert communications, this paper maximizes the minimum covert throughput from UAV to GRs, which can be formulated as an optimization problem with the constraints of covertness, UAV trajectory, power and user-association. We further simplify the optimization problem by determining the optimal transmission power of UAV. To solve this optimization problem, we derive the optimal transmission power of UAV and user-association index as analytical expressions of UAV's positions, respectively. We also define UAV trajectory as a successive hovering-and-flying structure. Based on these results, we employ a successive convex approximation method to obtain the maximum value of the minimum covert throughput. The numerical results are presented to illustrate the impact of system parameters on the minimum covert throughput.**

***Index Terms*—Unmanned aerial vehicle(UAV), covert communication, trajectory optimization, interweave cognitive radio network**

This work was supported in part by the National Natural Science Foundation of China under Grant 62372076, in part by the Yunnan Provincial Major Science and Technology Special Program under Grant 202602AC080004, in part by the Yunnan Key Laboratory of Cross-border Digital Economy under Grant 2025RD4916CE340007, in part by the Education Department Research Foundation of Anhui Province under Grant DTR2023051, in part by the Innovation Research Team on Future Network Technology of Chuzhou University, in part by the Innovation Team on Smart Home Appliance Security and Applications of Chuzhou City, in part by the Innovative Research Team on Application of Big Data and Financial Technology of Chuzhou University, in part by the Federal Ministry of Research, Technology, and Space (BMFTR), Germany, through the Project 6GEM+ under Grant 16KIS2411, in part by the European Union Horizon Europe research and innovation programme under the 6G-Path project under Grant 101139172.(Corresponding authors: Bin Yang; Shikai Shen).

Riyu Wang is with the School of Information Engineering, Kunming University, Kunming 650214, Yunnan, China (email: 943546889@qq.com).

Bin Yang is with the School of Computer and Information Engineering, Chuzhou University, Chuzhou 239000, Anhui, China (e-mail: yangbinchi@gmail.com).

Shikai Shen is with the School of Electronic Information and Automation, Dianchi College, Kunming 650228, Yunnan, China, the School of Information Engineering, Kunming University, Kunming 650214, Yunnan, China, and also with the Yunnan Key Laboratory of Intelligent Logistics Equipment and Systems, Kunming 650214, Yunnan, China(e-mail: kmssk2000@sina.com).

Yumei She is with the School of Mathematics and Computer Science, Yunnan Minzu University, Kunming 650200, Yunnan, China (e-mail: sheym1965@126.com).

Fei Deng is with the School of Information Engineering, Kunming University, Kunming 650214, Yunnan, China (email: feigeofffce@kmu.edu.cn).

Kaiguo Qian is with the School of Information Engineering, Kunming University, Kunming 650214, Yunnan, China (email: 769981805@qq.com).

Tarik Taleb is with the Faculty of Electrical Engineering and Information Technology, Ruhr University Bochum, 44801 Bochum, Germany (e-mail: tarik.taleb@rub.de).

I. INTRODUCTION

INTERWEAVE cognitive radio networks (ICRNs) are a cutting-edge network technique in the fifth-generation (5G) wireless communication system and beyond [1][2], where secondary users transmit data to their desired receivers using idle spectrum allocated to primary users, and thus improving the utilization efficiency of scarce spectrum resources. In particular, unmanned aerial vehicle (UAV) assisted ICRNs exhibit many promising features of flexible deployment, high mobility and low cost. They can support large number of sensitive data transmissions in various Internet of Things (IoT) applications [3]-[5], such as e-Health, emergency rescue and video monitoring. However, the sensitive data in such networks are highly susceptible to illegal eavesdropping attacks because of high quality air-to-ground channel and the broadcast nature of wireless signals. Secure communication is a technique to protect the transmitted content from being eavesdropped by malicious node. However, the transmission itself can still be detected. Covert communication is emerging as an important security technique, which hides the wireless communication process utilizing the randomness of wireless channels rather than high computational complexity like traditional cryptographic techniques [6]-[11]. In ICRN applications such as military scenarios, if an adversary detects the transmission, it may identify the communicating nodes and launch further attacks. Therefore, for supporting these security-sensitive applications, it is critical to explore covert communications in UAV-assisted ICRNs. Covert communications are emerging as an important security technique, which hides the wireless communication process utilizing the randomness of wireless channels rather than high computational complexity like traditional cryptographic techniques [6]-[11]. For supporting these security-sensitive IoT applications, it is critical to explore covert communications in UAV-assisted ICRNs.

Available works on covert communications mainly focus on two scenarios with and without UAV [12]-[28] (see Section II for details). For the scenario without UAV [12]-[19], these works explore various covertness scheme to enhance covert performances (e.g., covert throughput,covertness) based on noise uncertainty, channel uncertainty, and friendly jamming in single hop and two hop wireless systems. As for the scenario with UAV [20]-[28], these works jointly optimize UAV's trajectory and transmission power to improve covert performances, where UAV serves as either relay, aerial user or aerial base station. Recently, the works in [29]-[34] conduct some initial studies on covert communications in UAV-assisted ICRNs, where a UAV serves a single user. Specifically, the work in [29] maximized the effective throughput by a joint optimization of sensing blocklength, transmission blocklength, transmission power and UAV flight altitude. The work in [30] jointly optimized UAV trajectory and transmission power to maximize the covert rate using a model-driven generative adversarial network. The work in [31] maximized covert rate performance by jointly optimizing UAV location, transmission power, sensing time ratio and jamming power of a secondary receiver in the presence of multiple Wardens. Reference [32] proposed a cognitive radio system where a UAV with a reconfigurable intelligent surface acts as a relay and friendly jammer. The work employs optimization and deep learning to maximize covert throughput while adapting dynamically to environmental conditions. The work in [33] proposed a cognitive jamming-assisted cooperative UAV covert communication scheme. It maximizes the minimum average covert rate by alternately optimizing the jammer's sensing time and trajectory, as well as the transmitter's power and trajectory. Reference [34] proposed leveraging the primary user's signal as beneficial interference to disrupt warden detection. Under finite blocklength constraints, it formulates an average effective throughput maximization problem by jointly optimizing the UAV's transmit power and trajectory.

Note that the above works on the UAV covert communication in ICRNs consider that the primary user is legitimate, and an illegitimate user attempts to detect the communication process of the legitimate primary user. Moreover, the works consider that a UAV serves a single user. However, a UAV usually serves multiple users as well in practice. In such a multiple users' scenario, UAV trajectory and transmission power can significantly affect the covert performance between the UAV and each user. Different from the works, this paper focuses on a hybrid adversarial-cooperative scenario, where the primary user (Warden) operates under a dual identity. Publicly, the Warden serves as a legitimate member of the UAV's system and is therefore required to share its transmission schedule and channel state information to maintain its covert identity, which allows the UAV to be aware of the Warden's spectrum occupancy. Privately, the Warden is an illegitimate user to detect whether the UAV communicates with ground receivers (GRs). This scenario is common in applications such as military communications. For example, a terminal may present itself as a legitimate operational node, exchanging information with authorized users according to established protocols. However, privately, it acts as a spy by monitoring communication activities among legitimate users, enabling it to assess whether forces are operating in coordination and to infer the overall operational situation. In addition, this paper considers that a UAV can serve multiple users. In such a multiple users' scenario, UAV trajectory and transmission power can significantly affect the covert performance between the UAV and each user. Meanwhile, the UAV also needs to identify the user who communicates with it each time (i.e., user-association). To the best of our knowledge, this is the first work to jointly optimize the UAV trajectory, power and user-association to improve the covert performance in UAV-assisted ICRNs. Specifically, this paper explores the maximization of minimum covert throughput to ensure the covertness, timeliness and fairness of short-packet transmissions. The main contributions of this paper are summarized as follows.

(1) We concern on a UAV-assisted ICRN, which is comprised of a secondary user (UAV), multiple GRs, and a primary user Warden. UAV attempts to covertly transmit short-packets to GRs utilizing idle spectrum resource allocated to Warden. Warden detects the existence of UAV covert communications. To maximize the minimum covert throughput, we formulate it as a nonlinear nonconvex optimization problem with the constraints of covertness, UAV trajectory, power and user-association. We further simplify the optimization problem by determining the optimal transmission power of UAV.

(2) To solve the optimization problem, we derive the optimal transmission power of UAV and user-association index as analytical expressions of UAV's positions, respectively. Then, we construct the structure of the UAV trajectory, and transform the variables on an infinite number of trajectory points into these on a finite number of trajectory points for the optimization problem. Meanwhile, we obtain the minimum covert throughput relating the variables on discrete trajectory points through integration. We further use the successive convex approximation (SCA) method to approximate the optimization problem as a convex problem, and propose an iterative algorithm to solve it.

(3) Extensive numerical results are presented to illustrate the impacts of system parameters on minimum covert throughput and also to reveal our findings.

The rest of this paper is organized: In the Section II, we introduce related work on covert communication. In Section III, we present system model. In Section IV, we formulate optimization problem and further simplify this optimization problem. In Section V, we construct the optimal UAV flight trajectory structure. Further, we reformulate and solve the optimization problem in Section VI. Sections VII and Sections VIII provide numerical results and conclude this paper, respectively. Table 1 lists all the symbols used in this article and their corresponding explanations.

II. Related Work

A. Scenarios without UAV Assistance

In wireless network scenarios without UAV assistance, Hu et al. proposed a covert communication scenario in a relay network, where the relay attempts to covertly transmit its own information to the destination, while the source tried to detect this covert transmission. The authors proposed two strategies for the relay to transmit its covert information, namely rate-control and power control schemes, and derived achievable effective covert rates from the relay to destination [12]. Wang et al. proposed an IoT multi-antenna covert communication strategy based on spectral masking [13]. In [14], the authors considered a covert communication system with a Random Frequency Diversity Array at the transmitter Alice. Lin et al. studied the covert performance of limited blocklength device-to-device transmissions between multi-antenna transceivers assisted by Decode-and-Forward relay nodes [15]. In [16], due to the randomness of channel coefficients caused by multipath

TABLE I: All symbols and their explanations in the article

Symbol	Definition
K	Number of ground receivers
$\mathcal{K}$	Set of ground receivers, $\mathcal{K} = \{1, 2, \ldots, K\}$
$\mathbf{w}_k$	Position of the k-th GR
$\mathbf{w}_d$	Position of the Warden
$\hat{\mathbf{w}}_j$	Estimated position of GR or Warden
$\Delta\mathbf{w}_j$	Position uncertainty of GR or Warden
I	Total flight duration of the UAV
$\mathbf{q}(i)$	Horizontal position of UAV at time i
$\mathbf{q}_0$	Initial position of UAV
$\mathbf{q}_E$	Final position of UAV
H	UAV flight altitude
$h_k(i)$	Channel power gain from UAV to GR k at time i
$h_d(i)$	Channel power gain from UAV to Warden at time i
β_0	Channel power gain at unit distance
σ_k^2	AWGN power at GR k
σ_d^2	AWGN power at Warden
$a_k(i)$	User-association index
$\mathbf{a}(i)$	User-association vector: $(a_1(i), \ldots, a_K(i))$
$P(i)$	UAV transmission power at time i
$P_{\max}$	Maximum UAV transmission power
V	Maximum UAV speed
B	Channel bandwidth
$y_k(i)$	Received signal at GR k at time i
$y_d(i)$	Received signal at Warden at time i
H_0	Null hypothesis: UAV not transmitting
H_1	Alternative hypothesis: UAV transmitting
$\mathbb{P}_0, \mathbb{P}_1$	Likelihood functions under H_0 and H_1
$D(\mathbb{P}_1 \| \mathbb{P}_0)$	Kullback–Leibler divergence from $\mathbb{P}_1$ to $\mathbb{P}_0$
ρ_d	Covertness threshold
L	Blocklength of communication
$\dot{\mathbf{q}}(i)$	Velocity of UAV (first derivative of $\mathbf{q}(i)$)
R	Auxiliary variable: minimum covert throughput
λ	Average packet generation rate at Warden
ΔT_f	Average interval between two adjacent packets at Warden
T_f	Packet transmission duration for Warden
τ	Spectrum hole duration
P_{r_c}	Packet collision probability
P_{r_e}	Packet error probability
D	Amount of information sent by UAV
R^*	Transmission rate at UAV
γ_k	Signal-to-noise ratio at GR k
ψ, ϑ	Parameters in packet error probability expression
$\overline{\zeta}$	Average effective spectral efficiency
$\overline{P_{r_e}}$	Average packet error probability
L^*	Optimal blocklength
$p(\mathbf{q}(i))$	Optimal transmission power as function of position
$\mathbf{Q}$	Set of UAV trajectory points
$\mathbf{i}$	Vector of hovering durations
$d_{m,n}(\mathbf{Q})$	Distance between two adjacent trajectory points
$d_k(\mathbf{q})$	Distance from point $\mathbf{q}$ to GR k including altitude
$\theta_{m,k}^{(r)}$	Convex approximation of throughput at hovering point
$\Delta\tau$	Normalized time variable for flight phase
g	Number of iterations
$\epsilon_k^2, \epsilon_d^2$	Variance of position uncertainty for GR and Warden
$\mathbf{s}$	Set of feasible UAV flight paths

small-scale fading and Poisson channels, channel path loss and environmental noise were utilized to introduce confusion and mislead eavesdroppers. Ta et al. analyzed the impact of channel and noise uncertainty on Wardens during detection and derived covert performance considering channel and fading uncertainty [17]. In [18], the authors investigated the covert throughput maximization by jointly optimizing transmission power and blocklength of transmission and sensing in ICRNs. The goal of [19] was to maximize the spectral efficiency by jointly optimizing transmission power and blocklength of transmission in ICRNs.

B. Scenarios with UAV Assistance

Recent research has also focused on covert communications in wireless networks with the assistance of UAVs. In [20], the authors optimized the coding rate, transmission power, and the required number of hops to maxmize the throughput in a multi-hop network. Zhou et al. proposed a Penalty Sequence Convex Programming algorithm to improve system performance [21]. Building on this, Yan et al. considered covert communication scenarios enabled by UAVs, taking advantage of ground noise uncertainty, and designed the UAV's flight altitude and transmission power to conceal its transmission behavior [22]. In [23], the authors explored multi-UAV covert communication systems and proposed a random method based on Rapidly-exploring Random Tree to construct UAV trajectories under collision constraints. Furthermore, Wu et al. proposed a continuous hovering flight trajectory structure to optimize UAV trajectories [24]. Reference [25] introduced a UAV three-dimensional trajectory and intelligent reflecting surfaces (IRS) phase optimization algorithm based on dual deep networks to optimize UAV trajectories for the best covert communication performance. Wang et al. combined UAVs with IRS to propose a UAV-IRS-assisted covert communication scheme aimed at maximizing covert transmission rates [26]. Yang et al. proposed a dual-UAV-assisted covert communication system [27]. The paper in [28] investigated a covert communication system enabled by a fluid antenna array in the presence of an active warden. The authors maximized the minimum average covert rate by jointly optimizing the beamforming vectors, the autonomous aerial vehicle trajectory, and fluid antenna positions.

Note that the differences between our work and the references in [19] and [24] are summarized as follows. One key difference is that our work considers a hybrid adversarial-cooperative scenario. In contrast, the existing works in references assume a purely adversarial-noncooperative scenario, in which the adversarial detector does not cooperate with the legitimate users. Another difference is that the work in [24] focused on a multi-user UAV covert communication system but does not incorporate interweave spectrum sharing or cognitive-radio constraints; while the work in [19] examined interweave cognitive networks but only considers a single secondary transmitter-receiver pair, without UAV mobility or multi-user scheduling. Moreover, the difference scenarios also lead to different problem formulations and solution approaches. Our work derives the optimal transmission power and the user-association index as explicit functions of the UAV's position, and determine that the optimal trajectory follows a successive hover-and-fly structure. Furthermore, our work also transforms the original non-convex problem into a tractable form via discretized trajectory point parameterization and solve it using a SCA method tailored to our integrated constraints. In contrast, the work in [24] jointly optimize UAV trajectory and power allocation but do not incorporate cognitive-radio aspects, lacking corresponding collision analysis; while the work in [19] focuses on blocklength and power optimization in a fixed geometric setting, without considering trajectory or multi-user factors. In addition, regarding the similarity in trajectory structure, both our work and the work in [24] adopt the successive hovering and flying structure pattern. Our trajectory structure accounts for the impact of cognitive radio-related constraints, such as blocklength and packet collision probability, on the trajectory. In contrast, Reference [24] only considers the impact of transmit power and power allocation coefficient on the trajectory, without incorporating the impact of cognitive radio-related constraints.

For a comprehensive overview of research on covert communications in interweave cognitive radio networks [29]-[34], the typical system model consists of a primary legitimate transmitter, a secondary transmitter UAV, one or multiple wardens, and one or multiple receivers. In such scenarios, the secondary user UAV typically leverages the primary user's signa or activity patterns as beneficial interference or cover to conduct covert communications with the receivers. After deriving the minimum detection error probability or the Kullback–Leibler (KL) divergence, joint optimization of trajectory and power control, cooperative jamming strategies, or deep learning-based adaptive resource allocation is employed to achieve covert communication. However, in our study, we consider a distinct adversarial yet cooperative scenario where the UAV, acting as a secondary user, attempts to covertly deliver confidential information to GRs during its flight from an initial position to an end destination. The Warden has a dual identity, i.e., legitimate primary user in public and illegitimate user in private. Publicly, it pretends to be affiliated with the same group as the UAV, transmitting legitimate information to GRs. Privately, it acts as an illegitimate user to detect whether the UAV communicates with GRs. In public, the Warden must share its channel state information with the UAV to conceal its identity as an illegitimate user.

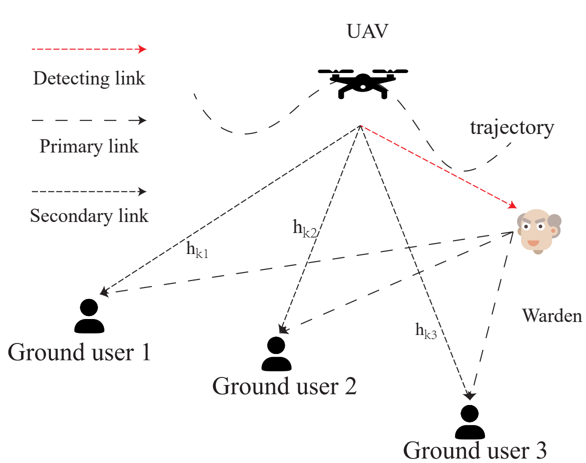

Fig. 1: Network model.

III. System Model

A. Network Model

As illustrated in Fig.1, the system consists of a UAV transmitter, a ground transmitter (Warden), and K GRs. The UAV acts as a secondary user, which attempts to covertly deliver confidential information to GRs during its flight from an initial position to an end position. The Warden has a dual identity, i.e., legitimate primary user in public, and illegitimate user in private. Publicly, it pretends to be affiliated with the same group as the UAV, transmitting legitimate information to GRs. Privately, it is an illegitimate user to detect whether the UAV communicates with GRs. In public, the warden needs to share its channel state information with the UAV to conceal its identity as an illegitimate user. The primary user Warden delivers information to GRs using primary spectrum and also detects the existence of wireless communications between UAV and GRs simultaneously. There exist three types of links, i.e., primary link from Warden to each GR, secondary link from UAV to each GR, and detecting link from UAV to Warden. These links use the primary spectrum. UAV can communicate with each GR when the primary spectrum is idle. Warden is equipped with a transmitting antenna and a receiving antenna, and each of other nodes is equipped with an antenna.

In two-dimensional Cartesian coordinate system,the position of the k-th GR is denoted by $\mathbf{w}_k = (w_{x,k}, w_{y,k}), \forall k \in \mathcal{K} \triangleq \{1, 2, \cdots, K\}$, and the position of the Warden is denoted by $\mathbf{w}_d = (w_{x,d}, w_{y,d})$. Actually, we may not have exact knowledge of the locations of GRs and Warden. Then, we represent $\mathbf{w}_j = \hat{\mathbf{w}}_j + \triangle\mathbf{w}_j, j \in \{k, d\}$, where $\hat{\mathbf{w}}_j = (\hat{w}_{x,j}, \hat{w}_{y,j}), j \in \{k, d\}$ denotes the estimated position of the k-th GR or Warden. Meanwhile, $\triangle\mathbf{w}_j = (\triangle w_{x,j}, \triangle w_{y,j}), j \in \{k, d\}$ denotes the uncertainty of the location of the k-th GR or Warden. We consider that $\triangle w_{x,j}$ and $\triangle w_{y,j}$ are independent and identically distributed (i.i.d.) Gaussian random variables. We use I to denote the flight duration of UAV from the initial point $\mathbf{q}_0 = (x_0, y_0)$ to the end point $\mathbf{q}_E = (x_E, y_E)$ on a horizontal plane parallel to the ground at a height of H.

B. Channel Model

We assume that the wireless channels from UAV to GRs are modeled as the free-space path loss channel for the unobstructed line-of-sight (Los) signal. We also assume that the wireless channels from Warden to GRs follow Rayleigh fading [24]. Since the Warden has a dual identity, it has to cooperative with the UAV in public, and thus the UAV knows the Warden's channel state information (CSI) and its location. Meanwhile, the background noise at all receivers is modeled as additive white Gaussian noise (AWGN). We use $h_k(i)$ and $h_d(i)$ to denote the channel gains from UAV to the k-GR and to Warden, respectively. Then,

$$h_k(i) = \sqrt{\frac{\beta_0}{\|\mathbf{q}(i) - \mathbf{w}_k\|^2 + H^2}}, h_d(i) = \sqrt{\frac{\beta_0}{\|\mathbf{q}(i) - \mathbf{w}_d\|^2 + H^2}}, \tag{1}$$

where $\|\mathbf{q}(i) - \mathbf{w}_j\|$ represents the Euclidean norm of $\mathbf{q}(i) - \mathbf{w}_j, j \in \{k, d\}$, β_0 is the channel gain per unit distance, $\mathbf{q}(i)$ denotes the horizontal position coordinates of UAV at time i, and $\mathbf{w}_j$ is a circularly symmetric complex Gaussian (CSGN) random variable following $\mathcal{CN}(q+H, \epsilon_j^2), j \in \{k, d\}$.

We use the user-association index $a_k(i)$ to represent whether or not UAV communicates with the k-th GR. When UAV does not communicate with the k-th GR, $a_k(i) = 0$. Otherwise, $a_k(i) = 1$. At each time i, UAV serves as one GR. Thus, we have

$$0 \leq a_k(i) \leq 1, \forall k \in \mathcal{K}, \tag{2}$$

and

$$\sum_{k=1}^{K} a_k(i) = 1, i \in [0, I]. \tag{3}$$

We use $\mathbf{a}(i)$ to represent the vector $(a_1(i), \ldots, a_K(i))$. In the flight duration I, the total throughput $R_k(\mathbf{q}(i), \mathbf{a}(i), P(i))$ between UAV and the k-th GR is determined as

$$\begin{aligned} & R_k(\mathbf{q}(i), \mathbf{a}(i), P(i)) \\ & = \int_0^I B \log_2 (1 + \frac{\beta_0 a_k(i) P(i)}{\sigma_k^2 (\|\mathbf{q}(i) - \mathbf{w}_k\|^2 + H^2)}) di, \end{aligned} \tag{4}$$

where σ_k^2 is the AWGN power and $P(i)$ denotes the transmission power of UAV at time i.

IV. Problem Formulation and Simplification

In this section, we formulate the maximization of minimum covert throughput as an optimization problem with the constraints of the UAV trajectory, power and user-association. We further simplify it by determining the optimal transmission power of UAV.

A. Problem Formulation

When the UAV transmits confidential information to the k-th GR at time i, the received signal $y_k(i)$ at the GR k is expressed as

$$y_k(i) = \sqrt{P(i)} h_k(i) x(i) + \sigma_k^2, \tag{5}$$

where $x(i)$ denotes the signal transmitted by the UAV at time i. Similarly, the received signal $y_d(i)$ at the Warden is expressed as

$$\begin{cases} y_d(i) = \sigma_d^2, & H_0, \\ y_d(i) = \sqrt{P(i)} h_d(i) x(i) + \sigma_d^2, & H_1, \end{cases} \tag{6}$$

where H_0 is the null hypothesis, indicating that the UAV is not transmitting information to the GRs, and H_1 is the alternative hypothesis, indicating that the UAV is communicating with the GRs. Likewise, σ_d^2 is the AWGN power.

The Warden performs optimal hypothesis testing and determines whether the UAV is communicating with the GRs based on the test results. Specifically, if the UAV is not communicating with the GRs and Warden decides on H_1, it is considered a false alarm. Conversely, if the UAV is communicating with the GRs and the Warden decides on H_0, it is considered a miss detection. According to [35], the covertness constraint is given by

$$\sqrt{D(\mathbb{P}_1 \,||\, \mathbb{P}_0)} \leq \sqrt{2} \rho_d, \tag{7}$$

where ρ_d is a covertness threshold, $\mathbb{P}_0$ and $\mathbb{P}_1$ represent the likelihood functions with H_0 and H_1, respectively, and $D(\mathbb{P}_1 \,||\, \mathbb{P}_0)$ represents the KL divergence from $\mathbb{P}_1$ to $\mathbb{P}_0$. Based on [36], we can further transform $D(\mathbb{P}_1 \,||\, \mathbb{P}_0)$ into

$$\mathcal{D}(\mathbb{P}_1 \| \mathbb{P}_0) = L \left[\frac{P(i) \left| h_d(i) \right|^2}{\sigma_d^2} - \ln \left(1 + \frac{P(i) \left| h_d(i) \right|^2}{\sigma_d^2} \right) \right], \tag{8}$$

where L denotes the blocklength of communication between the UAV and the GRs.

By substituting (8) into (7), and then performing a Taylor expansion, we obtain that

$$\begin{aligned} & \sqrt{L \left[\frac{P(i) \left| h_d(i) \right|^2}{\sigma_d^2} - \frac{P(i) \left| h_d(i) \right|^2}{\sigma_d^2} + \frac{1}{2} \left(\frac{P(i) \left| h_d(i) \right|^2}{\sigma_d^2} \right)^2 \right]} \\ & = \sqrt{\frac{1}{2} L \left(\frac{P(i) \left| h_d(i) \right|^2}{\sigma_d^2} \right)^2} \\ & \leq \sqrt{2} \rho_d. \end{aligned} \tag{9}$$

This approximation is justified because in covert communications, the transmission power is strictly constrained, resulting in low signal-to-noise ratio (SNR) $[\frac{P(i)|h_d(i)|^2}{\sigma_d^2}] \ll 1$. Under this low SNR, higher-order terms in the Taylor expansion become negligible. Retaining only the second-order term yields a convex quadratic constraint, which is essential for applying SCA methods efficiently. Similar low-order Taylor approximations are commonly adopted in related covert communication literature [24][27][29], in which first-order or second-order expansions are used to maintain tractability while preserving sufficient accuracy under low SNR conditions. Therefore, the Taylor expansion in Eq. (9) retains only the second-order term.

The objective of this paper is to jointly optimize UAV trajectory, UAV transmission power, and user-association index to maximize the minimum covert throughput between the UAV and the GRs, while satisfying the constraints of covertness and mobility. The optimization problem can be formulated as

$$\begin{aligned} (\text{OP}): \max_{\{\mathbf{q}(i)\}, \{\mathbf{a}(i)\}, \{P(i)\}} \; & \min_k R_k(\mathbf{q}(i), \mathbf{a}(i), P(i)) && \text{(10a)} \\ \text{s.t.}: \quad & \mathbf{q}(0) = \mathbf{q}_0, \mathbf{q}(I) = \mathbf{q}_E, && \text{(10b)} \\ & \left\| \dot{\mathbf{q}}(i) \right\|^2 \leq V^2, \forall i \in [0, I], && \text{(10c)} \\ & P(i) \leq P_{max}, \forall i \in [0, I], && \text{(10d)} \\ & (2), (3), (9), \end{aligned}$$

where $\dot{\mathbf{q}}(i)$ represents the first derivative of $\mathbf{q}(i)$ respect to i, V is the maximum flight speed of the UAV and P_{max} is the maximum transmission power. Constraint (10b) is the position constraint of the UAV, where the initial and final points are fixed. Constraint (10c) is the speed constraint of the UAV, which means that the maximum speed of the UAV's flight cannot exceed V. Constraint (10d) is the upper bound constraint on the transmission power of UAV. To facilitate our subsequent analysis, we introduce an auxiliary variable

R, representing the minimum covert throughput between the UAV and GR k. Furthermore, we can reformulate (OP) as

$$\text{(P1)}: \max_{\{\mathbf{q}(i)\},\{\mathbf{a}(i)\},\{P(i)\},R} R \tag{11a}$$
$$\text{s.t.}: \quad R_k(\mathbf{q}(i),\mathbf{a}(i),P(i)) \geq R, \forall k \in \mathcal{K}, \tag{11b}$$
$$\mathbf{q}(0)=\mathbf{q}_0, \mathbf{q}(I)=\mathbf{q}_E, \tag{11c}$$
$$\left\|\dot{\mathbf{q}}(i)\right\|^2 \leq V^2, \forall i \in [0,I], \tag{11d}$$
$$P(i) \leq P_{max}, \forall i \in [0,I], \tag{11e}$$
$$(2),(3),(9).$$

To solve this optimization problem with multiple variables, we will simplify the problem by deriving the optimal transmission power of UAV as analytical expression of users' positions in the next subsection.

B. Problem Simplification

The primary user Warden transmits data packets intermittently. Similar to [19], the average interval time ΔT_f for transmitting two adjacent packets at Warden is given by

$$\Delta T_f = \int_0^\infty t\lambda e^{-\lambda t} dt = \frac{1}{\lambda}, \tag{12}$$

where λ denotes the average packet generation rate at Warden. Then, the occupancy of band for Warden is given by $\rho = T_f\lambda$, where T_f denotes the packet transmission duration for Warden. We can express the probability that T_f is less than the spectrum hole duration τ as

$$Pr\left\{T_f < \tau\right\} = e^{-\lambda\tau}. \tag{13}$$

Meanwhile, the packet transmission duration T_f equals to L/B. Here, B denotes the bandwidth. The packet collision probability Pr_c is defined as the probability that both the primary user Warden and the secondary user UAV transmit information, simultaneously. Then, we have

$$Pr_c = Pr\left\{\tau < \frac{L}{B}\right\} = 1 - e^{-\frac{\lambda L}{B}}. \tag{14}$$

In communication processes, both packet collisions and packet transmission errors occur. Therefore, we introduce the transmission rate $R^* = D/L$, where D denotes the amount of information sent by UAV. The packet error probability is defined as the probability that the GR k receives an incorrect packet. Furthermore, according to [19], we can express the packet error probability as

$$Pr_e \approx \begin{cases} 1, & \gamma_k < \vartheta + \frac{1}{2\psi}, \\ \psi(\gamma_k - \vartheta) + \frac{1}{2}, & \vartheta + \frac{1}{2\psi} \leq \gamma_k \leq \vartheta - \frac{1}{2\psi}, \\ 0, & \gamma_k > \vartheta - \frac{1}{2\psi}, \end{cases} \tag{15}$$

where $\psi = -\sqrt{L/[2\pi(\exp(2R^*)-1)]}$,$\vartheta = \exp(R^*) - 1$, and $\gamma_k = P(i)\left|h_k(i)\right|^2/\sigma_k^2$ represents the SNR of GR k.

The average effective spectral efficiency (AESE) is the average rate of successfully delivered useful information per unit bandwidth per second. We will maximize the following AESE $\bar{\zeta}$ to improve the covertness performance, which is given by

$$\bar{\zeta} = \frac{T_f R^*}{2\Delta T_f}(1-Pr_c)(1-\overline{Pr}_e), \text{s.t.}(9) \text{ and } L \in \mathcal{Z}^+, \tag{16}$$

where $T_f/(2\Delta T_f)$ denotes the average number of times per unit time that the secondary user successfully initiates a transmission, $\overline{Pr}_e$ denotes average packet error probability, which will be elaborated in the following subsection, and $L \in \mathcal{Z}^+$ denotes that the blocklength is a positive integer.

Considering that both the blocklength and transmission power are independent variables of AESE, they have a significant impact on AESE. Therefore, this subsection will focus on optimizing the blocklength and transmission power to maximize AESE.

According to formulas (15) and (16), we observe that $\bar{\zeta}$ is a monotonically increasing function of $P(i)$, and $P(i) \leq 2\rho_d\sigma_d^2/(\sqrt{L}\left|h_d(i)\right|^2)$. Furthermore, we can obtain $P(i) = 2\rho_d\sigma_d^2/(\sqrt{L}\left|h_d(i)\right|^2)$ to satisfy the covertness constraint in (16) while maximizing AESE. Next, the corresponding average packet error probability is derived in the following lemma.

Lemma 1: The average packet error probability for transmitting a fixed amount of information D is given by

$$\overline{Pr}_e = 1 - \frac{2\sigma_d^2\epsilon_d^2\rho_d\psi}{\sqrt{L}\sigma_k^2\epsilon_k^2}\ln\left(1 + \frac{2\sqrt{L}\sigma_k^2\epsilon_k^2}{4\sigma_d^2\epsilon_d^2\rho_d\psi + \sqrt{L}\sigma_k^2\epsilon_k^2 z_2}\right), \tag{17}$$

where $z_1 = 2\vartheta\psi + 1$ and $z_2 = 2\vartheta\psi - 1$.

Proof: Please find the detailed proof in Appendix A. ■

To facilitate subsequent calculations, we simplify the average packet collision probability. Due to the strict concealment constraints, the transmission rate is very small. Therefore, using a Taylor expansion, we approximate the following variable as $\psi \approx -L/(2\sqrt{\pi D})$, $\vartheta \approx D/L$, $z_1 \approx -\sqrt{D/(4\pi)} + 1$ and $z_2 \approx -\sqrt{D/(4\pi)} - 1$. Thus, the average packet error probability can be further expressed as

$$\tilde{\overline{Pr}}_e \approx \frac{\sigma_k^2\sqrt{\pi D}\epsilon_k^2(\sqrt{D/(4\pi)}+1)}{2\sigma_d^2\epsilon_d^2\rho_d\sqrt{L} + \sigma_k^2\sqrt{\pi D}\epsilon_k^2(\sqrt{D/(4\pi)}+1)}. \tag{18}$$

Furthermore, based on (14) and (18), we can rewrite (16) as

$$\bar{\zeta} = \frac{\lambda D e^{-\frac{\lambda L}{B}}}{2B}(1 - \tilde{\overline{Pr}}_e), \text{s.t.} L \in \mathcal{Z}^+. \tag{19}$$

According to (18) and (19), we can obtain that AESE is a cubic equation with respect to blocklength. Therefore, we can determine the optimal blocklength to achieve the best AESE using the following lemma.

Lemma 2: The optimal blocklength L^* is given by

$$L^* = \left\lfloor \left(\sqrt[3]{\frac{\Theta B}{8\sigma_d^2\epsilon_d^2\rho_d\lambda} + \sqrt{\Delta}} + \sqrt[3]{\frac{\Theta B}{8\sigma_d^2\epsilon_d^2\rho_d\lambda} - \sqrt{\Delta}} \right)^2 \right\rfloor, \tag{20}$$

where $\lfloor * \rfloor$ represents the function that rounds $*$ down to the nearest integer, $\Theta = \sigma_k^2\sqrt{\pi D}\epsilon_k^2(\sqrt{D/(4\pi)}+1)$ and $\Delta = (\frac{\Theta B}{8\sigma_d^2\epsilon_d^2\rho_d\lambda})^2 + (\frac{\Theta}{6\sigma_d^2\epsilon_d^2\rho_d})^3$.

Proof: Please find the detailed proof in Appendix B. ■

Based on the optimal blocklength provided by Lemma 2, we can determine the optimal transmission power by substituting it into (9). Furthermore, the optimization equation (P1) can be rewritten as

$$\text{(P2)}: \max_{\{\mathbf{q}(i)\},\{\mathbf{a}(i)\},R} R \tag{21a}$$

$$\text{s.t.}: \int_0^I B\log_2(1+\frac{\beta_0 a_k(i)p(\mathbf{q}(i))}{\sigma_k^2(\|\mathbf{q}(i)-\mathbf{w}_k\|^2+H^2)})di \geq R, \forall k\in\mathcal{K}, \tag{21b}$$

$$(2),(3),(11c),(11d),$$

where $p(\mathbf{q}(i)) = \min(P_{max}, \frac{2\rho_d\sigma_d^2}{(\sqrt{L^*}|h_d(i)|^2)})$.

V. UAV Flight Trajectory Structure Design

In this section, we construct the optimal flight trajectory for UAV. Then, we prove that the successive hover-and-flying structure is the optimal trajectory structure. For the user-association index $\mathbf{a}(i)$, we can prove through Lemma 3 that it is a function of $\mathbf{q}(i)$.

Lemma 3: When the UAV follows the same path or hovers at a point, the coefficient $\mathbf{a}(i)$ does not change with time. Therefore, $\mathbf{a}(i)$ can be reconstructed as a function of $\mathbf{q}(i)$.

Proof: Please find the detailed proof in Appendix C. ■

According to Lemma 3, we can rewrite $\mathbf{a}(i)$ as $\mathbf{a}(\mathbf{q}(i))$. For convenience in subsequent analysis, we divide the total communication task duration I between the UAV and GRs into N segments, where N is a very large number and $\tau'' = I/N$. During each time τ'', the UAV either flies at a constant speed v' or hovers in a point. Additionally, for any UAV trajectory from the starting point $\mathbf{q}_0$ to the ending point $\mathbf{q}_E$, the flight process can be divided into three parts.

- Case 1 : When the UAV hovers at a certain point during the time τ'', its speed $v' = 0$. We use $\{\hat{\mathbf{q}}(i)\}$ to represent the entire trajectory points of the UAV task, where $\{\hat{\mathbf{q}}(i)\}$ has the same hovering point and the whole length of portion τ'' as its hovering duration.
- Case 2 : When the UAV flies at its maximum speed, the speed $v' = V$. We use $\{\bar{\mathbf{q}}(i)\}$ to represent the path of the UAV flying at maximum speed throughout the entire task, with each segment of the flight sustaining.
- Case 3 : We assume that the UAV flies at a speed v' throughout the entire duration, where $0 \leq v' \leq V$. Meanwhile, the flight time for each time is $\tau'' = \frac{\|\mathbf{q}_E(i)-\mathbf{q}_0(i)\|}{v'}$. Furthermore, we define the time during which the UAV flies at maximum speed as $\bar{\tau}'' = \frac{\|\mathbf{q}_E(i)-\mathbf{q}_0(i)\|}{V}$. The remaining time is denoted as $\hat{\tau}'' = \tau'' - \bar{\tau}''$. During the time $\hat{\tau}''$, the UAV flies at a speed of $\frac{Vv'}{V-v'}$.

Based on the above three cases, we can express (21a) as (22) (See the top of the this page). By (22), we can see that flying at a speed $0 \leq v' \leq V$ can be reconstructed as the sum of the paths $\{\hat{\mathbf{q}}(i)\}$ and $\{\bar{\mathbf{q}}(i)\}$. Therefore, the entire flight trajectory of the UAV can be optimized for the successive hovering and flying structure, where $i_1 = \frac{v'i}{V}$ and $i_2 = \frac{(V-v')i}{V}$. Based on the above derivation, we can transform formula (21a) into

$$\begin{aligned}&\int_0^I B\log_2(1+\frac{\beta_0 a_k(i)p(\mathbf{q}(i))}{\sigma_k^2(\|\mathbf{q}(i)-\mathbf{w}_k\|^2+H^2)})di \\ &= \int_0^{\bar{I}} B\log_2(1+\frac{\beta_0 a_k(\bar{\mathbf{q}}(i))p(\bar{\mathbf{q}}(i))}{\sigma_k^2(\|\bar{\mathbf{q}}(i)-\mathbf{w}_k\|^2+H^2)})di \\ &+ \int_0^{\hat{I}} B\log_2(1+\frac{\beta_0 a_k(\hat{\mathbf{q}}(i))p(\hat{\mathbf{q}}(i))}{\sigma_k^2(\|\hat{\mathbf{q}}(i)-\mathbf{w}_k\|^2+H^2)})di,\end{aligned} \tag{23}$$

where $\bar{I}$ represents the time the UAV flies at maximum speed V, and $\hat{I} = I - \bar{I}$.

Based on the above derivation, we can conclude that the minimum covert throughput between the UAV and GRs can be divided into the maximum flight speed phase and the unrestricted flight speed phase. According to (23), we can reformulate the optimization problem (P2) as

$$\text{(P3)}: \max_{\{\mathbf{q}(i)\},R} R \tag{24a}$$

$$\begin{aligned}\text{s.t.}: &\int_0^{\bar{I}} B\log_2(1+\frac{\beta_0 a_k(\bar{\mathbf{q}}(i))p(\bar{\mathbf{q}}(i))}{\sigma_k^2(\|\bar{\mathbf{q}}(i)-\mathbf{w}_k\|^2+H^2)})di \\ &+ \int_0^{\hat{I}} B\log_2(1+\frac{\beta_0 a_k(\hat{\mathbf{q}}(i))p(\hat{\mathbf{q}}(i))}{\sigma_k^2(\|\hat{\mathbf{q}}(i)-\mathbf{w}_k\|^2+H^2)})di \\ &\geq R, \forall k\in\mathcal{K}\end{aligned} \tag{24b}$$

$$\{\hat{\mathbf{q}}(i)\} \in s, \forall i \in [0,\hat{I}], \tag{24c}$$

$$0 \leq a_k(\mathbf{q}(i)) \leq 1, \forall k\in\mathcal{K}, i\in[0,I], \tag{24d}$$

$$\sum_{k=1}^K a_k(\mathbf{q}(i)) = 1, \forall i\in[0,I], \tag{24e}$$

where s denotes any UAV flight path.

According to (24b), we note that when the UAV flies at maximum speed, its optimal throughput remains constant, i.e., $\{\bar{\mathbf{q}}(i)\}$ is part of the optimal trajectory. Therefore, we will prove in the following lemma that $\{\hat{\mathbf{q}}(i)\}$ represents a set of hovering points.

Lemma 4:The optimal $\{\hat{\mathbf{q}}(i)\}$ of problem (P3) represents a set of hovering points.

Proof: Please find the detailed proof in Appendix D. ■

According to the characteristics of the successive hovering-and-flying structure, it is clear that the UAV will hover as close to GRs as possible to maximize minimum covert throughput when in a hovering state. Therefore, we can conclude that the UAV will have no more than K hovering points. Therefore, the optimal trajectory satisfies the following two conditions: i) following the successive hovering-and-flying structure; ii) the number of hovering points is less than or equal to K. It is worth noting that, unlike traditional trajectory discretization structures, the successive hovering-and-flying structure uses integration to calculate the throughput of UAVs when flying at maximum speed with GRs. Therefore, under the successive hovering-and-flying structure, the throughput between UAV and GRs does not suffer from discretization errors due to the discretization process.

VI. Problem Reformulation and Solution

Since it is difficult to solve this infinite variable optimization problem, we reformulate the problem by introducing a series of turning points. The UAV can adjust its flight direction at

$$
\begin{aligned}
&\underbrace{\int_0^{\tau''} B\log_2\left(1+\frac{\beta_0 a_k\left(\mathbf{q}_0(i)+\frac{(\mathbf{q}_E(i)-\mathbf{q}_0(i))v'i}{\|\mathbf{q}_E(i)-\mathbf{q}_0(i)\|}\right)p\left(\mathbf{q}_0(i)+\frac{(\mathbf{q}_E(i)-\mathbf{q}_0(i))v'i}{\|\mathbf{q}_E(i)-\mathbf{q}_0(i)\|}\right)}{\sigma_k^2\left(\left\|\mathbf{q}_0(i)+\frac{(\mathbf{q}_E(i)-\mathbf{q}_0(i))v'i}{\|\mathbf{q}_E(i)-\mathbf{q}_0(i)\|}-\mathbf{w}_k\right\|^2+H^2\right)}\right)di}_{\{\mathbf{q}(i)\}}\\
&=\frac{v'}{V}\int_0^{\tau''} B\log_2\left(1+\frac{\beta_0 a_k\left(\mathbf{q}_0(i)+\frac{(\mathbf{q}_E(i)-\mathbf{q}_0(i))v'i}{\|\mathbf{q}_E(i)-\mathbf{q}_0(i)\|}\right)p\left(\mathbf{q}_0(i)+\frac{(\mathbf{q}_E(i)-\mathbf{q}_0(i))v'i}{\|\mathbf{q}_E(i)-\mathbf{q}_0(i)\|}\right)}{\sigma_k^2\left(\left\|\mathbf{q}_0(i)+\frac{(\mathbf{q}_E(i)-\mathbf{q}_0(i))v'i}{\|\mathbf{q}_E(i)-\mathbf{q}_0(i)\|}-\mathbf{w}_k\right\|^2+H^2\right)}\right)di\\
&+\frac{V-v'}{V}\int_0^{\tau''} B\log_2\left(1+\frac{\beta_0 a_k\left(\mathbf{q}_0(i)+\frac{(\mathbf{q}_E(i)-\mathbf{q}_0(i))v'i}{\|\mathbf{q}_E(i)-\mathbf{q}_0(i)\|}\right)p\left(\mathbf{q}_0(i)+\frac{(\mathbf{q}_E(i)-\mathbf{q}_0(i))v'i}{\|\mathbf{q}_E(i)-\mathbf{q}_0(i)\|}\right)}{\sigma_k^2\left(\left\|\mathbf{q}_0(i)+\frac{(\mathbf{q}_E(i)-\mathbf{q}_0(i))v'i}{\|\mathbf{q}_E(i)-\mathbf{q}_0(i)\|}-\mathbf{w}_k\right\|^2+H^2\right)}\right)di\\
&=\underbrace{\int_0^{\bar{\tau}''} B\log_2\left(1+\frac{\beta_0 a_k\left(\mathbf{q}_0(i)+\frac{(\mathbf{q}_E(i)-\mathbf{q}_0(i))Vi_1}{\|\mathbf{q}_E(i)-\mathbf{q}_0(i)\|}\right)p\left(\mathbf{q}_0(i)+\frac{(\mathbf{q}_E(i)-\mathbf{q}_0(i))Vi_1}{\|\mathbf{q}_E(i)-\mathbf{q}_0(i)\|}\right)}{\sigma_k^2\left(\left\|\mathbf{q}_0(i)+\frac{(\mathbf{q}_E(i)-\mathbf{q}_0(i))Vi_1}{\|\mathbf{q}_E(i)-\mathbf{q}_0(i)\|}-\mathbf{w}_k\right\|^2+H^2\right)}\right)di_1}_{\{\bar{\mathbf{q}}(i)\}}\\
&+\underbrace{\int_0^{\hat{\tau}''} B\log_2\left(1+\frac{\beta_0 a_k\left(\mathbf{q}_0(i)+\frac{(\mathbf{q}_E(i)-\mathbf{q}_0(i))\frac{Vv'}{V-v'}i_2}{\|\mathbf{q}_E(i)-\mathbf{q}_0(i)\|}\right)p\left(\mathbf{q}_0(i)+\frac{(\mathbf{q}_E(i)-\mathbf{q}_0(i))\frac{Vv'}{V-v'}i_2}{\|\mathbf{q}_E(i)-\mathbf{q}_0(i)\|}\right)}{\sigma_k^2\left(\left\|\mathbf{q}_0(i)+\frac{(\mathbf{q}_E(i)-\mathbf{q}_0(i))\frac{Vv'}{V-v'}i_2}{\|\mathbf{q}_E(i)-\mathbf{q}_0(i)\|}-\mathbf{w}_k\right\|^2+H^2\right)}\right)di_2}_{\{\hat{\mathbf{q}}(i)\}}\,.
\end{aligned}
\tag{22}
$$

these turning points at maximum flying speed. Furthermore, we obtain the UAV's reformulated flight trajectory, transforming the problem from one with infinite variables to one with finite variables. Finally, we solve the problem using the SCA method.

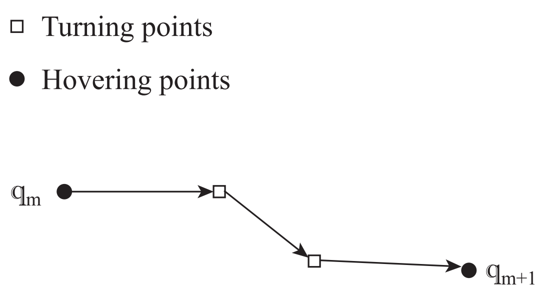

Fig. 2: Turning point diagram.

A. Problem Reformulation

According to the optimal UAV flight trajectory mentioned above, we first represent the m-th hovering point as $\mathbf{q}_m$, where $m \in \mathcal{K}$. Meanwhile, we set the hovering time of the UAV at hovering point m as t_m. Furthermore, we use the vector $\mathbf{i} = (i_1, \ldots, i_K)$ to denote the set of hovering durations. For problem (P3), we also need to calculate the throughput of the UAV during the maximum speed flight phase. Therefore, as shown in Fig. 2, we divide the trajectory between each pair of hovering points into $N+1$ segments, where N is the number of turning points and $\mathcal{N} \triangleq \{0, \ldots, N\}$. Thus, we can fit the UAV's trajectory with maximum speed using N turning points. To fit the trajectory of the UAV's entire task process, we set the trajectory between points $\mathbf{q}_m$ and $\mathbf{q}_{m+1}$ as $\mathbf{q}_{m,0}, \ldots, \mathbf{q}_{m,N+1}, m = 1, \ldots, K-1$. Accordingly, we will use $\mathbf{Q}$ to describe the UAV's entire task path, i.e.,

$$
\mathbf{Q} = [\mathbf{q}_{0,0}, \mathbf{q}_{0,1}, \ldots, \mathbf{q}_{0,N+1}, \mathbf{q}_{1,1}, \ldots, \mathbf{q}_{K,N+1}], \tag{25}
$$

where $\mathbf{q}_{0,0}$ denotes the initial point of UAV trajectory, and $\mathbf{q}_{K,N+1}$ denotes the ending point of UAV trajectory. The UAV will pass through all trajectory points along $\mathbf{Q}$ during the maximum speed flight phase.It is worth noting that increasing the number of turning points complicates the computation complexity but allows for a more accurate fit of the UAV's trajectory. Hence, we need to adjust the value of N to balance the fitting accuracy and computation complexity.

For convenience in subsequent analysis, we denote the distance between two adjacent points $\mathbf{q}_{m,n}$ and $\mathbf{q}_{m,n+1}$ on the trajectory as $d_{m,n}(\mathbf{Q}) = \|\mathbf{q}_{m,n+1} - \mathbf{q}_{m,n}\|$. Thus, we can obtain the relationship between $\mathbf{q}_{m,n}$ and $\mathbf{q}_{m,n+1}$ as follows

$$
\mathbf{q}_{m,n+1} = \mathbf{q}_{m,n} + \frac{(\mathbf{q}_{m,n+1} - \mathbf{q}_{m,n})Vi}{d_{m,n}(\mathbf{Q})}, i \in [0, \frac{d_{m,n}(\mathbf{Q})}{V}]. \tag{26}
$$

Additionally, due to this phase is the UAV's maximum speed flight phase, we have $\bar{\mathbf{q}}(i) = \mathbf{q}_{m,n+1}$.

Based on Lemma 3, we know that the user-association index $\mathbf{a}(i)$ is a function of $\mathbf{q}(i)$ only. Due to the trajectory points are constant within a set of UAV trajectories, we reconstruct $\mathbf{a}(i)$ as a series of constants and denote the user-association index at hover point $\mathbf{q}_m$ and on the flight segment $\mathbf{d_{m,n}}(\mathbf{q})$ for UAV communication with GR k as $a_{m,k}$ and $a_{m,n,k}$. Furthermore, we can express the throughput of the UAV communication with GR k as

$$\begin{aligned} R_k(\mathbf{Q},\mathbf{i},\mathbf{a}) &= \sum_{m=1}^{K} B\log_2(1+\frac{\beta_0 a_{m,k} p(\mathbf{q}_m)}{\sigma_k^2 d_k(\mathbf{q}_m)^2}) i_m \\ &+ \sum_{m=0}^{K}\sum_{n=0}^{N}\int_0^{\frac{d_{m,n}(\mathbf{Q})}{V}} B\log_2(1+\frac{\beta_0 a_{m,n,k} p(\bar{\mathbf{q}}_{m,n}(i))}{\sigma_k^2 d_k(\bar{\mathbf{q}}_{m,n}(i))^2}) di, \end{aligned} \tag{27}$$

where $d_k(\mathbf{q}) = \sqrt{\|\mathbf{q}-\mathbf{w}_k\|^2 + H^2}$ represents the distance from $\mathbf{q}$ to GR k. Meanwhile, (P3) can be reformulated as

$$(\text{P4}): \max_{\mathbf{Q},\mathbf{i},\mathbf{a},R} R \tag{28a}$$

$$\mathbf{s.t.}: \quad R_k(\mathbf{Q},\mathbf{i},\mathbf{a}) \geq R, \forall k \in \mathcal{K}, \tag{28b}$$

$$\sum_{m=1}^{K} i_m + \sum_{m=0}^{K}\sum_{n=0}^{N} \frac{d_{m,n}(\mathbf{Q})}{V} \leq I, \tag{28c}$$

$$\mathbf{i} \geq 0, \tag{28d}$$

$$0 \leq \mathbf{a} \leq 1, \sum_{k=1}^{K} a_{m,k} = 1, \sum_{k=1}^{K} a_{m,n,k} = 1, \quad \forall m \in \mathcal{K}, \forall n \in \mathcal{N}. \tag{28e}$$

We can observe that due to (27) is non-convex, which means (28b) is also non-convex, problem (P4) is non-convex as well. The optimization problem in (P4) established in this paper is highly non-convex and nonlinear, which makes it impossible to directly apply standard convex optimization tools to obtain the global optimal solution. For such non-convex problems, common optimization methods include branch-and-bound, heuristic algorithms, and iterative methods based on local convex approximation. Among these, branch-and-bound has low computational efficiency and cannot meet the quasi-real-time resource allocation requirements of covert communication systems. Heuristic algorithms cannot guarantee convergence to a specific optimal point. SCA offers an excellent balance between computational complexity and feasibility, along with well-defined theoretical convergence guarantees. In the next two subsection, we choose to adopt SCA to design an efficient solution algorithm.

B. Hovering Duration Convex Approximation

In this subsection, we use the SCA method to solve the UAV trajectory during the hovering phase. This allows us to determine the throughput $\theta_{m,k}^{(r)}(\mathbf{Q},\mathbf{i},\mathbf{a})$ for communication between the UAV at $\mathbf{q}_m$ and the GR k at each hovering point.

It is obvious that $f(x) = \log_2(1+x)$ is a concave function, and $f(\frac{1}{x}) = \log(1+\frac{1}{x})$ is also a concave function. Furthermore, for formulas $\log_2(1+\frac{\beta_0 a_{m,k} p(\mathbf{q}_m)}{\sigma_k^2 d_k(\mathbf{q}_m)^2}) i_m$, we can obtain the inequality at point $\mathbf{q}_m$ as follows

$$\log_2(1+\frac{\beta_0 a_{m,k} p(\mathbf{q}_m)}{\sigma_k^2 d_k(\mathbf{q}_m)^2}) i_m \geq -X_{m,k}^{(r)} \frac{d_k(\mathbf{q}_m)^2}{a_{m,k} p(\mathbf{q}_m)} i_m + Y_{m,k}^{(r)} i_m, \tag{29}$$

where $X_{m,k}^{(r)} = \frac{\beta_0 (a_{m,k}^{(r)})^2 p(\mathbf{q}_m^{(r)})^2}{(\sigma_k^2 d_k(\mathbf{q}_m^{(r)})^4 + \beta_0 (a_{m,k}^{(r)}) p(\mathbf{q}_m^{(r)}) d_k(\mathbf{q}_m^{(r)})^2)\ln 2}$ and $Y_{m,k} = \log_2(1+\frac{\beta_0 a_{m,k} p(\mathbf{q}_m)}{\sigma_k^2 d_k(\mathbf{q}_m)^2}) + X_{m,k}^{(r)} \frac{d_k(\mathbf{q}_m)^2}{p(\mathbf{q}_m)}$ are positive. According to the inequality involving the arithmetic mean, $\forall a_1,\ldots,a_M \in \mathcal{R}^+, a_1 a_2 \ldots a_M \leq (a_1^M +,\ldots,+ a_M^M)/M$, equality holds if and only if $a_1 =,\ldots,= a_M$. We can then derive

$$\begin{aligned} &- X_{m,k}^{(r)} \frac{d_k(\mathbf{q}_m)^2}{a_{m,k} p(\mathbf{q}_m)} i_m + Y_{m,k}^{(r)} i_m \\ &= -\frac{X_{m,k}^{(r)} d_k(\mathbf{q}_m)^2 (W_{1,m,k}^{(r)} W_{2,m,k}^{(r)} W_{3,m,k}^{(r)})}{(W_{1,m,k}^{(r)} W_{2,m,k}^{(r)} W_{3,m,k}^{(r)}) a_{m,k} p(\mathbf{q}_m)} i_m + Y_{m,k}^{(r)} i_m \\ &\geq -\frac{X_{m,k}^{(r)} \left(W_{1,m,k}^{(r)}\right)^3 d_k(\mathbf{q}_m)^8}{4 W_{2,m,k}^{(r)} W_{3,m,k}^{(r)}} - \frac{X_{m,k}^{(r)} \left(W_{2,m,k}^{(r)}\right)^3}{4 W_{1,m,k}^{(r)} W_{3,m,k}^{(r)} a_{m,k}^4} \\ &- \frac{X_{m,k}^{(r)} \left(W_{3,m,k}^{(r)}\right)^3}{4 W_{1,m,k}^{(r)} W_{2,m,k}^{(r)} p(\mathbf{q}_m)^4} - \frac{X_{m,k}^{(r)} i_m^4}{4 W_{1,m,k}^{(r)} W_{2,m,k}^{(r)} W_{3,m,k}^{(r)}} + Y_{m,k}^{(r)} i_m \\ &\triangleq \theta_{m,k}^{(r)}(\mathbf{Q},\mathbf{i},\mathbf{a}). \end{aligned} \tag{30}$$

According to the above inequality, we have $W_{1,m,k}^{(r)} = \frac{i_m^{(r)}}{d_k(\mathbf{q}_m^{(r)})^2}$, $W_{2,m,k}^{(r)} = i_m^{(r)} a_{m,k}^{(r)}$, and $W_{3,m,k}^{(r)} = i_m^{(r)} p(\mathbf{q}_m^{(r)})$. Equality holds if and only if the number of iterations r reaches its maximum. Thus, we obtain a convex approximation function for the throughput of the UAV communicating with the GR k at the hovering point $\mathbf{q}_m$, i.e. $\theta_{m,k}^{(r)}(\mathbf{Q},\mathbf{i},\mathbf{a})$ is the lower-bound concave function for the throughput at hovering point $\mathbf{q}_m$.

C. Flying Duration Convex Approximation

In this subsection, we use the SCA method to solve the UAV trajectory during the flying phase. This allows us to determine the throughput $\eta_{m,n,k}^{(r)}(\mathbf{Q},\mathbf{i},\mathbf{a})$ for communication between the UAV and the GR k along each segment of the flight path.

For the convenience of subsequent analysis, we introduce an auxiliary variable $\Delta\tau = \frac{Vi}{d_{m,n}(\mathbf{Q})}$. Based on the derivations from the previous subsection, we can construct the throughput for the flight phase as

$$\begin{aligned} &\int_0^{\frac{d_{m,n}(\mathbf{Q})}{V}} B\log_2\left(1+\frac{\beta_0 a_{m,n,k} p(\bar{\mathbf{q}}_{m,n}(i))}{\sigma_k^2 d_k\left(\bar{\mathbf{q}}_{m,n}(i)\right)^2}\right) di \\ &= \frac{d_{m,n}(\mathbf{Q})}{V}\int_0^1 B\log_2\left(1+\frac{\beta_0 a_{m,n,k} p(\bar{\mathbf{q}}'_{m,n}(\Delta\tau))}{K\sigma_k^2 d_k(\bar{\mathbf{q}}'_{m,n}(\Delta\tau))^2}\right) d\Delta\tau \\ &\geq \frac{d_{m,n}(\mathbf{Q})B}{V}\int_0^1 -X_{m,n,k}^{(r)}(\Delta\tau)\frac{d_k(\bar{\mathbf{q}}'_{m,n}(\Delta\tau))^2}{p(\bar{\mathbf{q}}'_{m,n}(\Delta\tau))} \\ &+ Y_{m,n,k}^{(r)}(\Delta\tau) d\Delta\tau \\ &= -\frac{d_{m,n}(\mathbf{Q})B}{V}\int_0^1 X_{m,n,k}^{(r)}(\Delta\tau)\frac{d_k(\bar{\mathbf{q}}'_{m,n}(\Delta\tau))^2}{a_{m,n,k} p(\bar{\mathbf{q}}'_{m,n}(\Delta\tau))} d\Delta\tau \\ &+ \frac{Z_{m,n,k}^{(r)}}{V} d_{m,n}(\mathbf{Q})B, \end{aligned} \tag{31}$$

where $\bar{\mathbf{q}}'_{m,n}(\Delta\tau) = \mathbf{q}_{m,n} + \Delta\tau(\mathbf{q}_{m,n+1} - \mathbf{q}_{m,n})$, $X_{m,n,k}^{(r)}(\Delta\tau) = X_{m,k}^{(r)}\big|_{\mathbf{q}_m^{(r)} = \bar{\mathbf{q}}_{m,n}'^{(r)}(\Delta\tau), a_{m,k}^{(r)} = a_{m,n,k}^{(r)}}$, $Y_{m,n,k}^{(r)}(\Delta\tau) = Y_{m,k}^{(r)}\big|_{\mathbf{q}_m^{(r)} = \bar{\mathbf{q}}_{m,n}'^{(r)}(\Delta\tau), a_{m,k}^{(r)} = a_{m,n,k}^{(r)}}$ and $Z_{m,n,k}^{(r)} = \int_0^1 Y_{m,n,k}^{(r)}(\Delta\tau) d\Delta\tau$ are all positive.

$$
\begin{aligned}
&-\frac{d_{m,n}(\mathbf{Q})B}{V}\int_0^1 X_{m,n,k}^{(r)}(\Delta\tau)\frac{d_k(\bar{\mathbf{q}}'_{m,n}(\Delta\tau))^2}{a_{m,n,k}p(\bar{\mathbf{q}}'_{m,n}(\Delta\tau))}d\Delta\tau+\frac{Z_{m,n,k}^{(r)}d_{m,n}(\mathbf{Q})B}{V}\\
&=-\frac{W_{1,m,n,k}^{(r)}W_{2,m,n,k}^{(r)}d_{m,n}(\mathbf{Q})B}{VW_{1,m,n,k}^{(r)}W_{2,m,n,k}^{(r)}a_{m,n,k}}\int_0^1 X_{m,n,k}^{(r)}(\Delta\tau)\frac{d_k(\bar{\mathbf{q}}'_{m,n}(\Delta\tau))^2}{a_{m,n,k}p(\bar{\mathbf{q}}'_{m,n}(\Delta\tau))}d\Delta\tau+\frac{Z_{m,n,k}^{(r)}}{V}d_{m,n}(\mathbf{Q})B\\
&\geq-\frac{\left(W_{1,m,n,k}^{(r)}\right)^2B}{3VW_{2,m,n,k}^{(r)}}\left(\int_0^1\frac{X_{m,n,k}^{(r)}(\Delta\tau)d_k(\bar{\mathbf{q}}'_{m,n}(\Delta\tau))^2}{p(\bar{\mathbf{q}}'_{m,n}(\Delta\tau))}d\Delta\tau\right)^3\\
&-\frac{\left(W_{2,m,n,k}^{(r)}\right)^2B}{3VW_{1,m,n,k}^{(r)}a_{m,n,k}^3}-\frac{d_{m,n}(\mathbf{Q})^3B}{3VW_{1,m,n,k}^{(r)}W_{2,m,n,k}^{(r)}}+\frac{Z_{m,n,k}^{(r)}d_{m,n}(\mathbf{Q})B}{V}\\
&=-\frac{\left(W_{1,m,n,k}^{(r)}\right)^2B}{3VW_{2,m,n,k}^{(r)}}\left(\int_0^1\frac{X_{m,n,k}^{(r)}(\Delta\tau)W_{3,m,n,k}^{(r)}(\Delta\tau)d_k(\bar{\mathbf{q}}'_{m,n}(\Delta\tau))^2}{W_{3,m,n,k}^{(r)}(\Delta\tau)p(\bar{\mathbf{q}}'_{m,n}(\Delta\tau))}d\Delta\tau\right)^3\\
&-\frac{\left(W_{2,m,n,k}^{(r)}\right)^2B}{3VW_{1,m,n,k}^{(r)}a_{m,n,k}^3}-\frac{d_{m,n}(\mathbf{Q})^3B}{3VW_{1,m,n,k}^{(r)}W_{2,m,n,k}^{(r)}}+\frac{Z_{m,n,k}^{(r)}}{V}d_{m,n}(\mathbf{Q})B\\
&\geq-\frac{\left(W_{1,m,n,k}^{(r)}\right)^2B}{3VW_{2,m,n,k}^{(r)}}\left(\int_0^1\frac{X_{m,n,k}^{(r)}(\Delta\tau)W_{3,m,n,k}^{(r)}(\Delta\tau)}{2p(\bar{\mathbf{q}}'_{m,n}(\Delta\tau))^2}+\frac{X_{m,n,k}^{(r)}(\Delta\tau)d_k(\bar{\mathbf{q}}'_{m,n}(\Delta\tau))^4}{2W_{3,m,n,k}^{(r)}(\Delta\tau)}d\Delta\tau\right)^3\\
&-\frac{\left(W_{2,m,n,k}^{(r)}\right)^2B}{3VW_{1,m,n,k}^{(r)}a_{m,n,k}^3}-\frac{d_{m,n}(\mathbf{Q})^3B}{3VW_{1,m,n,k}^{(r)}W_{2,m,n,k}^{(r)}}+\frac{Z_{m,n,k}^{(r)}d_{m,n}(\mathbf{Q})B}{V},
\end{aligned}
\tag{32}
$$

By following the inequality transformations from the previous subsection, we can obtain a convex approximation expression in (32) for the throughput from UAV to GR k during the flight phase (See the top of next page). In (32), $W_{1,m,n,k}^{(r)}=\frac{d_{m,n}(\mathbf{Q}^{(r)})}{\int_0^1 X_{m,n,k}^{(r)}(\Delta\tau)\frac{d_k(\bar{\mathbf{q}}'^{(r)}_{m,n}(\Delta\tau))^2}{p(\bar{\mathbf{q}}'^{(r)}_{m,n}(\Delta\tau))}d\Delta\tau}$, $W_{2,m,n,k}^{(r)}=d_{m,n}(\mathbf{Q}^{(r)})a_{m,n,k}^{(r)}$ and $W_{3,m,n,k}^{(r)}=d_k(\bar{\mathbf{q}}'^{(r)}_{m,n}(\Delta\tau))^2p(\bar{\mathbf{q}}'^{(r)}_{m,n}(\Delta\tau))$ are also all positive. Equality holds if and only if the number of iterations r reaches its maximum. Due to $d_{m,n}(\mathbf{Q})$ is a convex function of $(\mathbf{Q})$, we construct a concave approximation for $d_{m,n}(\mathbf{Q})$ as follows

$$
\begin{aligned}
d_{m,n}(\mathbf{Q})\geq&\frac{1}{d_{m,n}(\mathbf{Q}^{(r)})}(x_{m,n+1}^{(r)}-x_{m,n}^{(r)})(x_{m,n+1}-x_{m,n})\\
&+(y_{m,n+1}^{(r)}-y_{m,n}^{(r)})(y_{m,n+1}-y_{m,n})\\
\triangleq& d_{m,n}^{(r)}(\mathbf{Q}).
\end{aligned}
\tag{33}
$$

Furthermore, we can reformulate (32) as

$$
\begin{aligned}
&\eta_{m,n,k}^{(r)}(\mathbf{Q},\mathbf{i},\mathbf{a})\triangleq-\frac{\left(W_{1,m,n,k}^{(r)}\right)^2B}{3VW_{2,m,n,k}^{(r)}}(\int_0^1\frac{X_{m,n,k}^{(r)}(\Delta\tau)W_{3,m,n,k}^{(r)}(\Delta\tau)}{2p(\bar{\mathbf{q}}'_{m,n}(\Delta\tau))^2}\\
&+\frac{X_{m,n,k}^{(r)}(\Delta\tau)d_k(\bar{\mathbf{q}}'_{m,n}(\Delta\tau))^4}{2W_{3,m,n,k}^{(r)}(\Delta\tau)}d\Delta\tau)^3-\frac{\left(W_{2,m,n,k}^{(r)}\right)^2B}{3VW_{1,m,n,k}^{(r)}a_{m,n,k}^3}\\
&-\frac{d_{m,n}(\mathbf{Q})^3B}{3VW_{1,m,n,k}^{(r)}W_{2,m,n,k}^{(r)}}+\frac{Z_{m,n,k}^{(r)}d_{m,n}^{(r)}(\mathbf{Q})B}{V}.
\end{aligned}
\tag{34}
$$

Similar to the previous context, $\eta_{m,n,k}^{(r)}(\mathbf{Q},\mathbf{i},\mathbf{a})$ represents the throughput of the UAV communicating with GR k during the flight phase, and it is a lower-bound concave function. Combining (28b), (30) and (34), we obtain

$$
\begin{aligned}
R_k(\mathbf{Q},\mathbf{i},\mathbf{a})\geq&\sum_{m=1}^{K}\theta_{m,k}^{(r)}(\mathbf{Q},\mathbf{i},\mathbf{a})\sum_{m=0}^{K}\sum_{n=0}^{N}\eta_{m,n,k}^{(r)}(\mathbf{Q},\mathbf{i},\mathbf{a})\\
\triangleq& R_k^{(r)}(\mathbf{Q},\mathbf{i},\mathbf{a}).
\end{aligned}
\tag{35}
$$

where equality holds if and only if the number of iterations r reaches its maximum.

Based on the above derivation, we have approximated (P4) at point $(\mathbf{Q}^{(r)},\mathbf{i}^{(r)},\mathbf{a}^{(r)})$ as a convex form. Therefore, we can convert (P4) into

$$
(P5):\max_{\mathbf{Q},\mathbf{i},\mathbf{a},R} R \tag{36a}
$$

$$
\text{s.t.}:R_k^{(r)}(\mathbf{Q},\mathbf{i},\mathbf{a})\geq R,\forall k\in\mathcal{K}, \tag{36b}
$$

$$
(28c),(28d),(28e).
$$

So far, we have transformed the non-convex problem (OP) into a convex problem (P5). We can now solve it using convex optimization methods. Specifically, after solving the relaxed problem, we apply a simple rounding strategy where the user with the maximum association value is selected, i.e.,$a_k(i)=\begin{cases}1, & \text{if } k=\arg\max_j a_j(i),\\ 0, & \text{otherwise}\end{cases}$. This approach ensures feasibility while maintaining near-optimal performance. The value obtained after each iteration is used in the next iteration until the optimal solution is found. The specific algorithm is shown in Algorithm 1.

In the initialization of the position variable $\mathbf{Q}^{(0)}$, we adopt a simplified initialization method. The UAV initial trajectory is set as a straight line from the start point $\mathbf{q}_0$ to the end point $\mathbf{q}_E$, traversing K hovering points, without using any prior information of the ground receivers' locations. This makes the initialization method applicable to arbitrary user distributions. Although this initialization is simple, it is sufficient based on the SCA framework. In each iteration, even starting from a straight-line trajectory, the algorithm automatically adjust the trajectory to form hovering points near the ground receivers, because the objective function strongly penalizes long distances to any user. In the initialization of the position variable $\mathbf{a}^{(0)}$, for each hovering point $\mathbf{q}_m^{(0)}$, we associate it with the GR that has the smallest distance $d_k(\mathbf{q}_m^{(0)})$. That is, we set $a_{m,k}^{(0)} = 1$ for that k and 0 otherwise. This produces a binary association that satisfies $\sum_k a_{m,k} = 1$ and $a_{m,k} \in \{0, 1\}$. The same rule is applied to the flight phase association indices $a_{m,n,k}^{(0)}$. This initial association is both feasible and close to the expected optimal solution because the UAV tends to serve the nearest user when hovering. In the initialization of the position variable $\mathbf{i}^{(0)}$, the total mission time I is first allocated evenly among all hovering points and flight segments. Then, starting from an equal allocation, we slightly increase the duration of the hovering point corresponding to the GR with the currently lowest throughput, while decreasing the duration of the hovering point with the highest throughput, keeping the total time unchanged.

According to Algorithm 1, we analyze the complexity of the algorithm. Note that this algorithm is based on the ellipsoid method for solving, and its complexity is mainly related to the number of optimization variables and constraints in the optimization problem. For optimization problem (P5), it contains $N_v = K^2 I + 2K^2 + 3KI + 4K + 2I$ optimization variables and $N_c = (2K+1)(K + (K+1)(I+1)) + K + 1$ constraints. According to the complexity analysis in [38], in each iteration, the algorithm needs to introduce calculations for the quantities of N_v and N_c. Therefore, on the basis of the iteration number g, the complexity of Algorithm 1 is given as

$$\begin{aligned} &\mathcal{O}\left(gN_v^2\right) \times \left(\mathcal{O}\left(N_v\right)^2 \mathcal{O}\left(N_v N_c\right)\right) \\ &= \mathcal{O}\left(g\left(N_v^4 + N_v^3 N_c\right)\right). \end{aligned} \tag{37}$$

In Fig.3, we can observe that as the number of iterations increases, the minimum covert throughput gradually rises. When the number of iterations reaches 11, the value of the optimization objective essentially stabilizes. This indicates that our proposed algorithm converges efficiently to an optimal solution within a few iterations.

VII. Numerical Results

In this section, we evaluate the covert communication performance of interweave cognitive radio networks assisted by UAV. We set the default values for the parameters as: $K = 5$, $\beta = -140\,\mathrm{dBm}$, $B = 15\,\mathrm{kHz}$, $\lambda = 70$, $D = 4\,nats$, $H = 30\,\mathrm{m}$, $P_{max} = 20\,\mathrm{dBm}$, $I = 500\,s$, $V = 5\,\mathrm{m/s}$, $\epsilon_k^2 = \epsilon_d^2 = 25$, $\sigma_k^2 = \sigma_d^2 = -80\,\mathrm{dBm}$, $\rho_d = 0.05$, $N = 1$, $\mathbf{w}_d = (500, 600)$, $\mathbf{w}_k = [(220, 260), (360, 270), (910, 90), (780, 620), (870, 750)]$, $\mathbf{q}_0 = (100, 100)$ and $\mathbf{q}_E = (900, 900)$. The following figures, unless otherwise specified, will not change the parameters.

Algorithm 1 Solving the optimization problem in (P4)

Initailization

Initializing $(\mathbf{Q}^{(r)}, \mathbf{i}^{(r)}, \mathbf{a}^{(r)})$, and setting $r = 0$ and tolerance ϵ.

Iteration

Obtaining $R_k^{(r)}(\mathbf{Q}, \mathbf{i}, \mathbf{a})$ based on $(30), (34)$ and (35);
Solving the optimization problem in (P5) and obtaining the optimal local point $(\mathbf{Q}^*, \mathbf{i}^*, \mathbf{a}^*)$ and current optimal minimum covert throughput R^*;
if the difference between the current optimal minimum covert throughput and the previous one is no more than ϵ **then**
    Stop iteration;
else
    $(\mathbf{Q}^{(r)}, \mathbf{i}^{(r)}, \mathbf{a}^{(r)}) = (\mathbf{Q}^*, \mathbf{i}^*, \mathbf{a}^*)$;
    $r = r + 1$;
end if
return to 1;

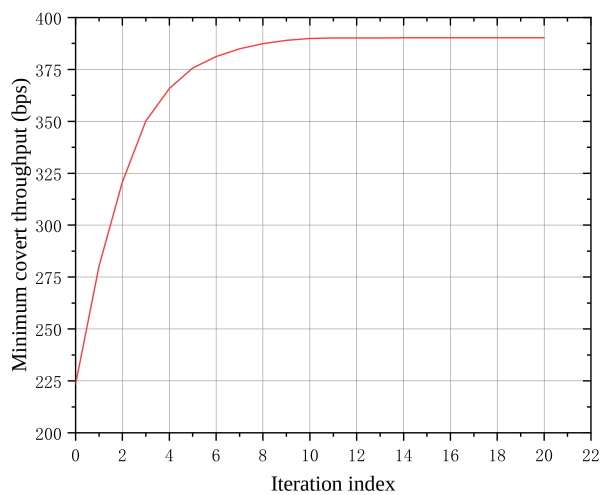

Fig. 3: Algorithm iteration diagram.

First, we analyze the UAV's flight trajectory. As shown in Fig. 4, the UAV takes off from the initial position and approaches the GRs along the shortest possible path while avoiding the Warden. Moreover, the UAV's hovering position should be as close to directly above the GRs as possible, which ensures the communication quality between the UAV and the GRs.

Meanwhile, the successive hover-and-flying structure balances communication quality and mobility cost, requiring the UAV to allocate mission time to locate favorable communication positions. Among these, hovering is the optimal strategy for fully exploiting a favorable location, allowing the UAV to dedicate continuous time blocks to high-quality transmission for individual users. Flying at the maximum speed V reduces the time needed for the UAV to reposition to

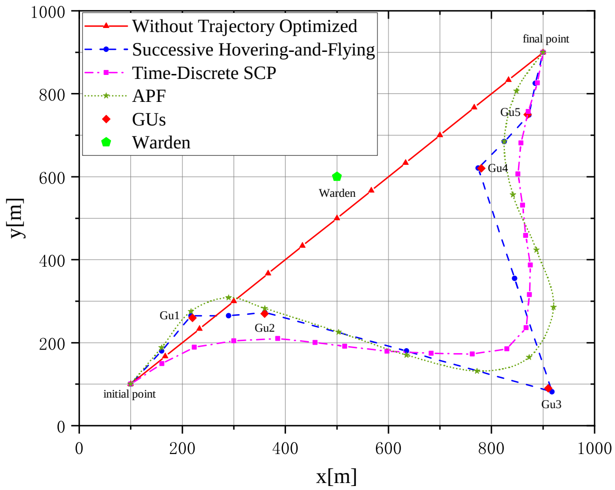

Fig. 4: The UAV trajectory.

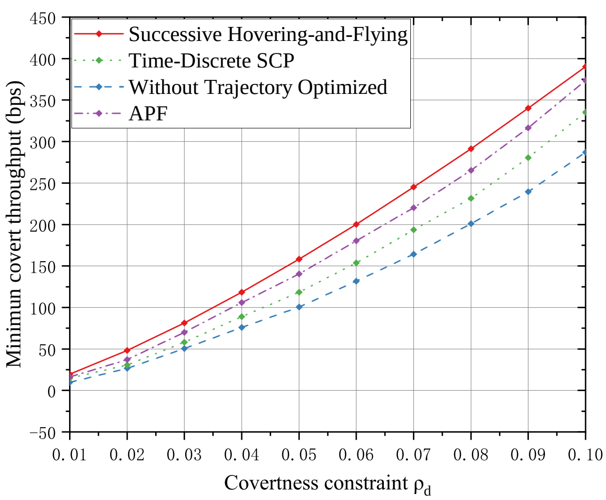

Fig. 5: Performance comparison under different flight structures.

advantageous locations, thereby maximizing the time available for actual data transmission and improving communication efficiency. We compare our adopted successive hover-and-flying trajectory structure with other flight strategies, i.e., time-discrete sequential convex programming (SCP)[24],the artificial potential field (APF) [39] and no trajectory optimization. Here, the APF scheme is interpreted as follows: when the mission time is sufficient, the optimal UAV trajectory exhibits a “hover and fly” structure: the UAV flies toward the point with the lowest potential field at maximum speed, hovers at that point to communicate at the maximum rate, and then flies to the destination at maximum speed. The time-discrete SCP discretizes the UAV flight trajectory into a large number of time slots and computes the covert throughput within each slot discretely, which will expend substantial computational power to simulate a continuous flight trajectory. In our work, we adopt the successive hovering-and-flying trajectory structure, where the flight path is divided into a series of flight segments with different constant speeds, and the covert throughput of each segment is obtained through integration, thus reducing the computational effort required. Fig. 5 illustrates their trajectories and performance comparation. As shown in Fig. 5, we can observe that for each fixed covertness constraint ρ_d, the minimum covert throughput performance under our trajectory structure, as well as under APF and time-discrete SCP, is better than that without trajectory optimization. In particular, our trajectory structure achieves a higher minimum covert throughput than both APF and time-discrete SCP.

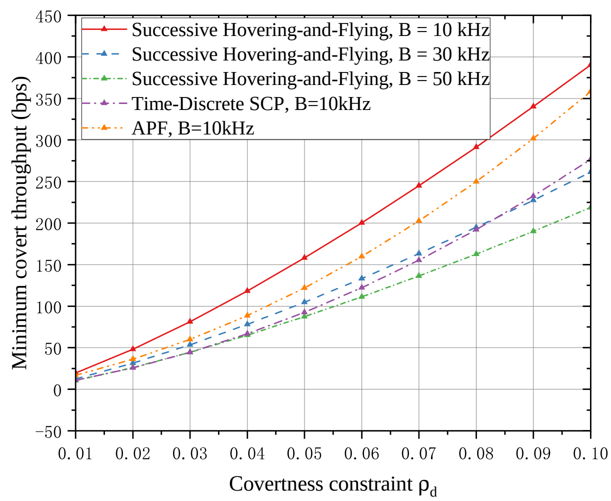

Fig. 6: The relationship between the covert constraint ρ_d and the minimum covert throughput for different channel bandwidths B.

As shown in Fig. 6, the minimum covert throughput between the UAV and the GRs increases as the ρ_d gradually increases. Conversely, when the B increases, the minimum covert throughput decreases. This is because a higher covert threshold relaxes the covert constraints, allowing the UAV to transmit information with higher power, resulting in better communication quality between the UAV and GRs. At the same time, smaller channel communication bandwidth leads to increased communication time between the Warden and GRs, prompting the UAV to adaptively adjust the blocklength to reduce the packet collision probability. As the packet collision probability decreases, the communication quality between the UAV and GRs improves, resulting in an increase in the minimum covert throughput. Therefore, we should choose a lower bandwidth for communication whenever possible, while still satisfying the covert constraints and maintaining communication quality. Meanwhile, when $B = 10kHz$, the minimum covert throughput under all three trajectory structures increases as ρ_d is relaxed. It is worth noting that, for a fixed ρ_d, our proposed trajectory structure exhibits superior performance.

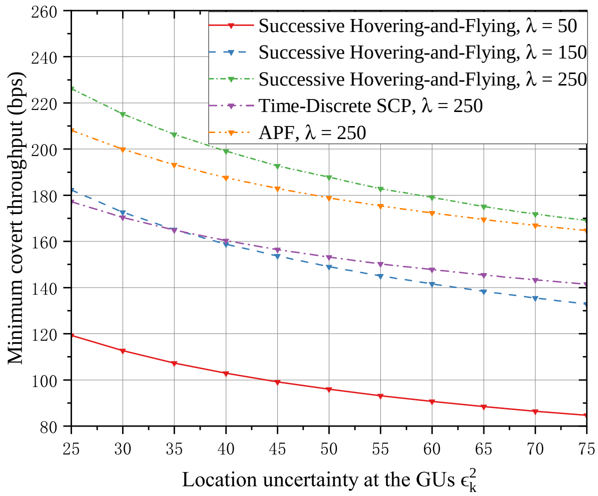

Fig. 7: The relationship between the location uncertainty ϵ_k^2 and the minimum covert throughput for different Warden's average packet generation rate λ.

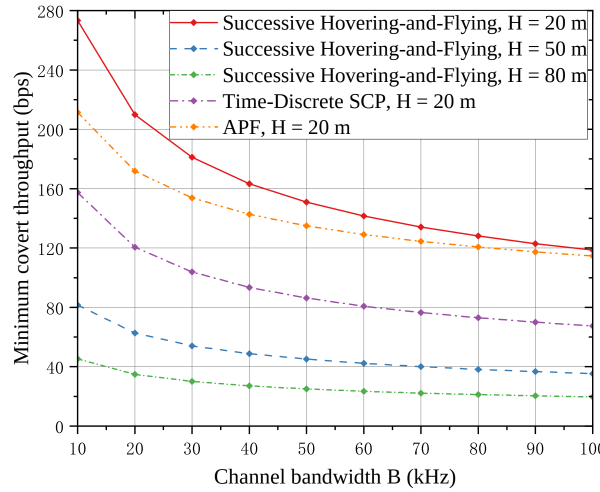

Fig. 8: The relationship between the channel bandwidths B and the minimum covert throughput for different UAV flight altitude H.

In Fig. 7, we discuss the impact of GRs location uncertainty ϵ_k^2 and the Warden's average packet generation rate λ on the minimum covert throughput. As ϵ_k^2 increases, the minimum covert throughput between the UAV and GRs decreases. Conversely, as the λ increases, the minimum covert throughput increases. This is because higher GRs location uncertainty enlarges the blocklength for UAV-to-GRs communication, leading to increased packet collision probability and reduced UAV transmission power, thus decreasing the minimum covert throughput. When the Warden's average packet generation rate increases, the UAV adaptively reduces the blocklength to avoid collisions with the Warden, which results in higher transmission power and increased minimum covert throughput. This indicates that we should aim to determine user locations as accurately as possible and not worry about the Warden increasing their communication frequency. Meanwhile, when λ=250, the minimum covert throughput under all three trajectory structures decreases as ϵ_k^2 becomes stricter. It is worth noting that, for a fixed ϵ_k^2, our proposed trajectory structure exhibits superior performance. Moreover, the APF structure significantly outperforms the discrete SCP structure.

Next, we discuss the impact of UAV flight altitude and bandwidth on the minimum covert throughput. As shown in Fig. 8, when the UAV flight altitude H increases, the minimum covert throughput decreases. This is because an increase in UAV flight altitude results in a longer distance between the UAV and GRs, leading to increased path loss and, consequently, reduced communication quality and minimum covert throughput. It is worth noting that when the UAV flight altitude is lower, changes in altitude have a more significant impact on the minimum covert throughput. As the altitude H increases, the effect on minimum covert throughput diminishes. This is because, at higher altitudes, the impact of path loss on communication quality gradually decreases. Meanwhile, when the bandwidth B is relatively small, its impact on the minimum covert throughput is more pronounced. As shown in Formula (20), a smaller bandwidth results in a shorter blocklength for the UAV's transmitted information. Meanwhile, according to the formula $P(i) = 2\rho_d \sigma_d^2/(\sqrt{L}|\ h_d(i)\ |^2)$, as the blocklength decreases, the UAV's transmit power increases. Thus, a smaller bandwidth leads to higher transmit power for the UAV, thereby improving the minimum covert throughput. When the bandwidth is small, an increase in bandwidth results in a relatively large change in magnitude, accompanied by a significant variation in the UAV's transmit power, which causes a noticeable change in the minimum covert throughput. As the bandwidth gradually increases, its impact on the minimum covert throughput progressively diminishes. This is because when the bandwidth is sufficiently large, the dominant factors limiting the blocklength gradually shift to other parameters such as λ and ρ_d, causing the variation in blocklength to slow down. Due to this reduced variation in blocklength, the change in transmit power also slows down, which in turn alleviates the influence of transmit power on the variation of the minimum throughput. Therefore, we should choose a lower bandwidth for communication whenever possible, while still satisfying the covert constraints and maintaining communication quality. When $H = 20m$, the minimum covert throughput under all three trajectory structures decreases as B is increased. It is worth noting that, for a fixed B, the performance of our trajectory structure and the APF trajectory structure is far superior to that of discrete SCP, and the performance under our trajectory structure is slightly better than that of APF.

In Fig. 9, we evaluate the impact of the Warden's average packet generation rate and variable versus fixed blocklength strategies on the minimum covert throughput. When the Warden's average packet generation rate increases, the UAV adaptively reduces the blocklength to avoid collisions with

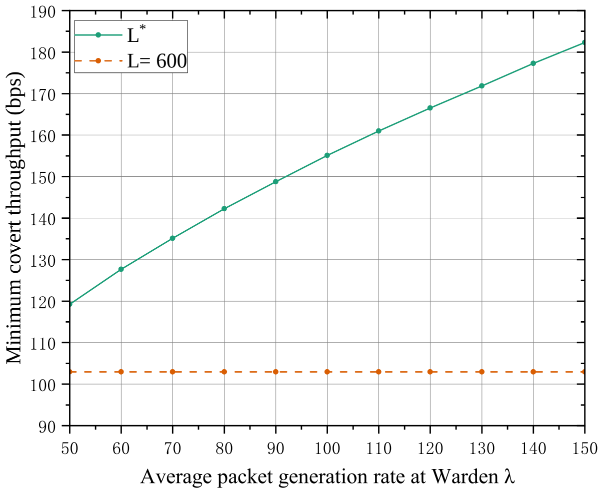

Fig. 9: The relationship between the Warden's average packet generation rate λ and the minimum covert throughput for different blocklength L setting strategy.

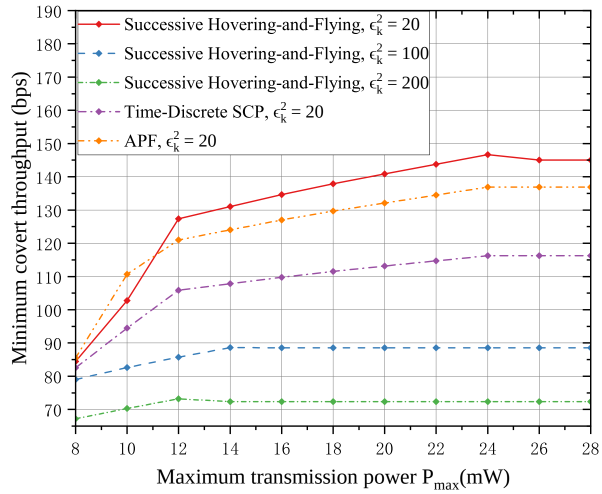

Fig. 10: The relationship between the maximum transmission power P_{max} and the minimum covert throughput for different location uncertainty ϵ_k^2.

the Warden, which results in higher transmission power and increased minimum covert throughput. This indicates that we should aim to determine user locations as accurately as possible and not worry about the Warden increasing their communication frequency. When L is fixed, the minimum covert throughput remains unchanged as the Warden's average packet generation rate increases. However, if L is optimized, the minimum covert throughput gradually increases as λ increases. As derived, when L is fixed, the UAV's transmission power $p(\mathbf{q}(i)) = \min(P_{max}, \frac{2\rho_d \sigma_d^2}{(\sqrt{L^*}|h_d(i)|^2)})$, and as long as the transmission power meets the covert constraints, the minimum covert throughput remains unaffected. If the UAV optimizes L, it will adaptively reduce L as λ increases to avoid packet collisions, which increases $p(\mathbf{q}(i))$ and consequently raises the minimum covert throughput. Thus, optimizing L is indeed meaningful.

As shown in Fig. 10, when P_{max} gradually increases, the minimum covert throughput first increases and then stabilizes. We have $p(\mathbf{q}(i)) = \min(P_{max}, \frac{2\rho_d \sigma_d^2}{(\sqrt{L^*}|h_d(i)|^2)})$. When P_{max} is less than $\frac{2\rho_d \sigma_d^2}{(\sqrt{L^*}|h_d(i)|^2)}$, $p(\mathbf{q}(i)) = P_{max}$, so as P_{max} increases, $p(\mathbf{q}(i))$ also increases, resulting in better communication quality and increased minimum covert throughput. When P_{max} exceeds $\frac{2\rho_d \sigma_d^2}{(\sqrt{L^*}|h_d(i)|^2)}$, $p(\mathbf{q}(i)) = \frac{2\rho_d \sigma_d^2}{(\sqrt{L^*}|h_d(i)|^2)}$, so $p(\mathbf{q}(i))$ remains constant as P_{max} increases. Additionally, as ϵ_k^2 increases in Fig. 10, the minimum covert throughput significantly decreases, further confirming that a larger ϵ_k^2 leads to reduced channel quality and thus lower minimum covert throughput. This is because higher GRs location uncertainty enlarges the blocklength for UAV-to-GRs communication, leading to increased packet collision probability and reduced UAV transmission power, thus decreasing the minimum covert throughput. Moreover, when $\epsilon_k^2 = 20$, the minimum covert throughput under all three trajectory structures increases with P_{max}. When P_{max} increases to a certain value, the minimum covert throughput remains unchanged. It is worth noting that, overall, the performance under our trajectory structure is better than that of APF and discrete SCP.

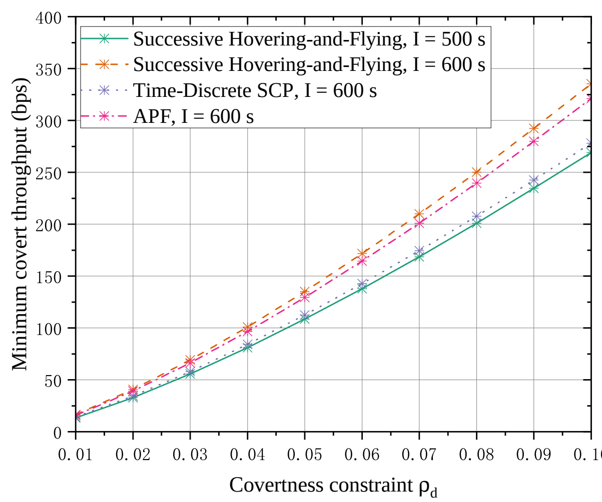

Fig. 11: The relationship between the covert constraint ρ_d and the minimum covert throughput for different task time I.

Finally, we discuss the impact of UAV task time I on the minimum covert throughput. In Fig. 11, as I increases, the minimum covert throughput also increases. This is because a longer I allows the UAV to better fit its flight path closer to the GRs, providing more time for communication and reducing path loss, which improves communication quality and thus increases the minimum covert throughput. However, it is important to note that when covert constraints are very strict, the impact of I on the minimum covert throughput is minimal, as these stringent constraints significantly reduce communication quality, making the effect of small changes in I negligible. When covert constraints are relaxed, the impact of I on the minimum covert throughput becomes significantly greater. As shown in Fig. 11, when $I = 600s$, the minimum covert throughput under all three trajectory structures decreases as ρ_d is relaxed. It is worth noting that, for a fixed ρ_d, the performance of our trajectory structure and the APF trajectory structure is far superior to that of discrete SCP, and the performance under our trajectory structure is slightly better than that of APF.

VIII. Conclusion

This paper investigated covert communications in UAV-assisted ICRNs, which aims to maximize the minimum covert throughput for ensuring the fairness of covert communications by a joint optimization of UAV trajectory, power and user-association. It was formulated as a nonlinear nonconvex optimization problem. To solve this problem, we derived the optimal transmission power of UAV and user-association index as analytical expressions of users' positions, respectively. We also designed the UAV trajectory structure. Then, we obtained the maximum value of the minimum covert throughput by a successive convex approximation method.The numerical results illustrated that a careful setting of parameters such as the transmission power, trajectory and blocklength of the UAV can significantly improve the minimum covert throughput. An interesting direction for future work is to analyze UAV spectrum sensing, particularly in non-cooperative communication scenarios where the UAV lacks prior knowledge of the Warden's spectrum holes. We further analyze the spectrum sensing in the successive hovering and flying structure.

References

[1] A. Ali and W. Hamouda, "Advances on Spectrum Sensing for Cognitive Radio Networks: Theory and Applications," *IEEE Commun. Surv. Tuts.*, vol. 19, no. 2, pp. 1277–1304, Nov. 2016.

[2] Y. Zou, J. Zhu, L. Yang, and Y.-C. Liang, "Securing Physical-Layer Communications for Cognitive Radio Networks," *IEEE Commun. Mag.*, vol. 53, no. 9, pp. 48–54, Sep. 2015.

[3] F. Liu et al., "Integrated Sensing and Communications: Toward Dual-Functional Wireless Networks for 6G and Beyond," *IEEE J. Sel. Areas Commun.*, vol. 40, no. 6, pp. 1728–1767, Mar. 2022.

[4] Y. Heng et al., "Six Key Challenges for Beam Management in 5.5G and 6G Systems," *IEEE Commun. Mag.*, vol. 59, no. 7, pp. 74–79, Jul. 2021.

[5] Y. Liu et al., "A Multi-Dimensional Intelligent Multiple Access Technique for 5G Beyond and 6G Wireless Networks," *IEEE Trans. Wireless Commun.*, vol. 20, no. 2, pp. 1308–1320, Oct. 2020.

[6] N. Wang, P. Wang, A. Alipour-Fanid, and K. Zeng, "Physical-Layer Security of 5G Wireless Networks for IoT: Challenges and Opportunities," *IEEE Internet Things J.*, vol. 6, no. 5, pp. 8169–8181, Jul. 2019.

[7] Q. Wu, W. Mei, and R. Zhang, "Safeguarding Wireless Network with UAVs: A Physical Layer Security Perspective," *IEEE Wireless Commun.*, vol. 26, no. 5, pp. 12–18, Oct. 2019.

[8] H. Guo, J. Liu, J. Ren, and Y. Zhang, "Intelligent Task Offloading in Vehicular Edge Computing Networks," *IEEE Wireless Commun.*, vol. 27, no. 4, pp. 126–132, Jun. 2020.

[9] H. Hartenstein and L. P. Laberteaux, "A Tutorial Survey on Vehicular Ad Hoc Networks," *IEEE Commun. Mag.*, vol. 46, no. 6, pp. 164–171, Jun. 2008.

[10] N. Yang et al., "Safeguarding 5G Wireless Communication Networks Using Physical Layer Security," *IEEE Commun. Mag.*, vol. 53, no. 4, pp. 20–27, Apr. 2015.

[11] Y. Zeng, R. Zhang, and T. J. Lim, "Wireless Communications with Unmanned Aerial Vehicles: Opportunities and Challenges," *IEEE Commun. Mag.*, vol. 54, no. 5, pp. 36–42, May. 2016.

[12] J. Hu et al., "Covert Communication Achieved by a Greedy Relay in Wireless Networks," *IEEE Trans. Wireless Commun.*, vol. 17, no. 7, pp. 4766–4779, May. 2018.

[13] P. Wan et al., "Spectrum Mask-Based Multi-Antenna Covert Communications in IoT Networks," *IEEE Trans. Cogn. Commun. Netw.*, vol. 10, no. 2, pp. 567–579, Nov. 2023.

[14] L. Li et al., "Covert Wireless Communication with Random Frequency Diverse Array," *IEEE Trans. Veh. Technol.*, vol. 73, no. 1, pp. 1473–1478, Sep. 2023.

[15] M. Lin et al., "DF-Relay-Assisted Multi-Antenna D2D Covert Communication in the Presence of Joint Detection," *IEEE Internet Things J.*, vol. 11, no. 7, pp. 11800–11811, Nov. 2023.

[16] L. Wang, "Covert Communication Over the Poisson Channel," *IEEE J. Sel. Areas Inf. Theory*, vol. 2, no. 1, pp. 23–31, Jan. 2021.

[17] H. Q. Ta et al., "Covert Communication with Noise and Channel Uncertainties," *Wireless Netw.*, vol. 28, no. 1, pp. 161–172, Nov. 2021.

[18] R. Xu et al., "Finite Blocklength Covert Communications in Interweave Cognitive Radio Networks," *IEEE Commun. Lett.*, vol. 26, no. 9, pp. 1989–1993, Jun. 2022.

[19] X. Lu et al., "Short-Packet Covert Communication in Interweave Cognitive Radio Networks," *IEEE Trans. Veh. Technol.*, vol. 72, no. 2, pp. 2649–2654, Sep. 2022.

[20] H. M. Wang et al., "Secrecy and Covert Communications Against UAV Surveillance via Multi-Hop Networks," *IEEE Trans. Commun.*, vol. 68, no. 1, pp. 389–401, Nov. 2019.

[21] S. Yan et al., "Hiding Unmanned Aerial Vehicles for Wireless Transmissions by Covert Communications," in *Proc. IEEE Int. Conf. Commun. (ICC)*, Jul. 2019. pp. 1–6.

[22] X. Zhou et al., "Three-Dimensional Placement and Transmit Power Design for UAV Covert Communications," *IEEE Trans. Veh. Technol.*, vol. 70, no. 12, pp. 13424–13429, Oct. 2021.

[23] H. Huang, A. V. Savkin, and W. Ni, "Navigation of a UAV Team for Collaborative Eavesdropping on Multiple Ground Transmitters," *IEEE Trans. Veh. Technol.*, vol. 70, no. 10, pp. 10450–10460, Aug. 2021.

[24] P. Wu et al., "Joint Power Allocation and Trajectory Design for UAV-Enabled Covert Communication," *IEEE Trans. Wireless Commun.*, vol. 23, no. 1, pp. 683–698, Jun. 2023.

[25] S. Bi et al., "Deep Reinforcement Learning for IRS-Assisted UAV Covert Communications," *China Commun.*, vol. 20, no. 12, pp. 131–141, May. 2023.

[26] C. Wang et al., "Covert Communication Assisted by UAV-IRS," *IEEE Trans. Commun.*, vol. 71, no. 1, pp. 357–369, Nov. 2022.

[27] G. Yang et al., "Covert Wireless Communications for Augmented Reality Systems with Dual Cooperative UAVs," *IEEE J. Sel. Topics Signal Process.*, vol. 17, no. 5, pp. 1119–1130, Jul. 2023.

[28] J. Wei et al., "Fluid Antenna Array-Enabled AAV Covert Communications Against Active Warden," *IEEE Trans. Wireless Commun.*, vol. 25, pp. 9030-9045, 2026.

[29] B. Wang et al., "Analysis and Optimization of UAV-Assisted Covert Communications in Interweave Cognitive Radio Networks," *IEEE Trans. Cogn. Commun. Netw.*, Jan. 2025.

[30] Z. Li et al., "MD-GAN-Based UAV Trajectory and Power Optimization for Cognitive Covert Communications," *IEEE Internet Things J.*, vol. 9, no. 12, pp. 10187-10199, Jun. 2022.

[31] J. Wei et al., "UAV Covert Communications in Interweave Cognitive Radio Network," *IEEE Trans. Cogn. Commun. Netw.*, May. 2025.

[32] V. Nhan Vo et al., "Deep Learning-Driven Throughput Maximization in Covert Communication for UAV-RIS Cognitive Systems," *IEEE Open J Commun Soc*, vol. 6, pp. 4140-4155, Apr. 2025.

[33] J. Wei et al., "Cognitive Jamming-aided UAV Multi-user Covert Communication," *JSAC*, pp. 1-1, Nov. 2025.

[34] Q. Wang et al, "UAV-Assisted Covert Transmission for Cooperative Cognitive Radio Networks," *IEEE Trans. Wireless Commun*, vol. 25, pp. 1594-1608, 2026.

[35] B. Bash, D. Goeckel, and D. Towsley, "Limits of Reliable Communication with Low Probability of Detection on AWGN Channels," *IEEE J. Sel. Areas Commun.*, vol. 31, no. 9, pp. 1921–1930, Aug. 2013.

[36] C. Wu, Y. Xiao, and P. Yang, "Covert Information Embedded Spatial Modulation," *IEEE Commun. Lett.*, vol. 24, no. 11, pp. 2426–2430, Jul. 2020.

[37] W. Yu and R. Lui, "Dual Methods for Nonconvex Spectrum Optimization of Multicarrier Systems," *IEEE Trans. Commun.*, vol. 54, no. 7, pp. 1310–1322, Jul. 2006.

[38] X. Yuan et al., “Trajectory Design for UAV-Enabled Multiuser Wireless Power Transfer with Nonlinear Energy Harvesting,” *IEEE Trans. Wireless Commun.*, vol. 20, no. 2, pp. 1105–1121, Oct. 2020.

[39] Y. Huang et al., “Analytical Optimal Joint Resource Allocation and Continuous Trajectory Design for UAV-Assisted Covert Communications,” *IEEE Trans. Wireless Commun*, vol. 24, no. 1, pp. 213-227, Jan. 2025.

[40] Y. Hu, X. Yuan, J. Xu, et al., “Optimal 1D Trajectory Design for UAV-Enabled Multiuser Wireless Power Transfer,” *IEEE Trans. Commun.*, vol. 67, no. 8, pp. 5674–5688, Apr. 2019.

Riyu Wang received the Bachelor’s degree in Internet of Things Engineering from Guangdong University of Petrochemical Technology in 2023. He is currently pursuing a master’s degree at Kunming University in Yunnan, China. His research interests include UAV-assisted wireless communication networks and cognitive radio networks.

Bin Yang received the Ph.D. degree in systems information science from Future University, Hakodate, Japan, in 2015. He was a Research Fellow with the School of Electrical Engineering, Aalto University, Espoo, Finland, from Nov. 2019 to Nov. 2021. He is currently a Professor with the School of Computer and Information Engineering, Chuzhou University, Chuzhou, China. His research interests include unmanned aerial vehicle networks, mobile edge computing, cyber security, and Internet of Things.

Shikai Shen received his B.S. and M.S. Degrees from Yunnan Normal University in 1984 and from Yunnan University in 2003, respectively. He is currently a Professor with the School of Electronic Information and Automation, Dianchi College, Kunming 650228, Yunnan, China, the School of Information Engineering, Kunming University, Kunming 650214, Yunnan, China, the Yunnan Key Laboratory of Intelligent Logistics Equipment and Systems, Kunming 650214, Yunnan, China, and also afffliated with the Academician Weiming Shen Workstation, Kunming 650214, Yunnan, China. He is also a Senior Member of the China Computer Federation. His research interests include wireless sensor networks, cyber security, the Internet of Things, etc.

Yumei She received the B.S. degree from Minzu University of China, Peking, China, in 1985. She is currently a Professor with the Yunnan Minzu University, and Yunnan Province Key Laboratory of Smart City and Cyberspace Security. Prof. She is a member of the China Computer Federation. Her research interests include natural language processing and wireless sensor networks.

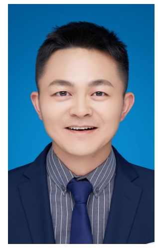

Fei Deng is currently pursuing a Ph.D. in artificial intelligence at Xi’an Jiaotong University. He received his B.Sc. and M.Sc. degrees from the Xi’an University of Science and Technology and the Guangxi University, respectively. He is currently a senior engineer with Kunming University. His current research interests include artificial neural networks and data mining.

Kaiguo Qian received his B.S. from Sichuan University in 2002 and M.S degrees from University of Electronic Science and Technology of China in 2010,respectively. He is currently a professor of School of Mechanical and Electrical Engineering, Kunming University, Yunnan, China, and also affiliated with the Academician Weiming Shen Workstation, Yunnan 650214, China. He is a member of the Yunnan Province Key Laboratory of Intelligent Logistics Equipment and Systems, China. He is also a Member of the China Computer Federation. His research interests include wireless sensor networks, cyber security,the Internet of Things, etc.

Tarik Taleb received the B.E. degree with distinction in Information Engineering and the M.Sc. and Ph.D. degrees in Information Sciences from Tohoku University, Sendai, Japan, in 2001, 2003, and 2005, respectively. He is currently a Full Professor at Ruhr University Bochum (RUB), Germany, where he leads research activities on next-generation mobile and distributed systems. Prior to joining RUB, he was a Professor at the University of Oulu, Finland (2018–2023), and an Associate Professor at Aalto University, Finland (2014–2021). Earlier in his career, he served as a Senior Researcher and 3GPP Standards Expert at NEC Europe Ltd., Heidelberg, Germany, where he contributed to the evolution of mobile network architectures and standardization activities. Before joining NEC, he was an Assistant Professor at the Graduate School of Information Sciences, Tohoku University, Japan, working in a research laboratory fully funded by KDDI. He also held a Research Fellowship at the Intelligent Cosmos Research Institute, Japan, from 2005 to 2006. Prof. Taleb is widely recognized for his pioneering contributions to mobile network softwarization, network slicing, cloud-edge continuum management, and autonomous networking. His current research interests include autonomous network and service management, edge-cloud continuum systems, network softwarization and slicing, software-defined security, and AI-native communication networks.